STUDIES ON SOME BRAIN MRI SEGMENTATION TECHNIQUES SUITABLE FOR ONLINE APPLICATIONS

Thesis submitted in partial fulfilment of the requirements for the degree of

MASTER of ELECTRICAL ENGINEERING

By

SHRAMANA GUHA SARKAR

REGISTRATION NO. - 128909 of 2014-15

ROLL NO. - M4ELE16-16

Under the guidance of

Dr. DEBANGSHU DEY

&

Prof. BISWAJIT BHATTACHARYYA

ELECTRICAL ENGINEERING DEPARTMENT

FACULTY COUNCIL OF ENGINEERING & TECHNOLOGY

JADAVPUR UNIVERSITY

KOLKATA-700032, INDIA

2016

JADAVPUR UNIVERSITY
FACULTY COUNCIL OF ENGINEERING & TECHNOLOGY
ELECTRICAL ENGINEERING DEPARTMENT
KOLKATA-700032, INDIA

CERTIFICATE of RECOMMENDATION

We hereby recommend that the thesis prepared under our supervision and guidance by **Shramana Guha Sarkar** entitled **"Studies on Some Brain MRI Segmentation Techniques Suitable for Online Applications"** be accepted in partial fulfilment of the requirements for award of the degree of **"Master of Electrical Engineering"** at **Jadavpur University**. The project, in our opinion, is worthy of acceptance.

SUPERVISORS

Dr. DEBANGSHU DEY
Assistant Professor
Electrical Engineering Department
Jadavpur University
Kolkata – 700032, India

Prof. BISWAJIT BHATTACHARYYA
Associate Professor
Electrical Engineering Department
Jadavpur University
Kolkata – 700032, India

COUNTERSIGNED

Dr. SWAPAN KUMAR GOSWAMI
Professor and Head of the Department
Electrical Engineering Department
Jadavpur University

Dr. SIVAJI BANDYOPADHYAY
Dean, **Faculty of Engg. & Tech.**
Jadavpur University
Kolkata – 700032, India

JADAVPUR UNIVERSITY
FACULTY COUNCIL OF ENGINEERING & TECHNOLOGY
ELECTRICAL ENGINEERING DEPARTMENT
KOLKATA-700032, INDIA

CERTIFICATE of APPROVAL*

The foregoing thesis is hereby approved as a creditable study of an engineering subject carried out and presented in a satisfactory manner to warrant its acceptance as a pre-requisite to the degree for which it has been submitted. It is notified to be understood that by this approval, the undersigned do not necessarily endorse or approve any statement made, opinion expressed and conclusion drawn therein but approve the thesis only for the purpose for which it has been submitted.

Final Examination for Evaluation of the Thesis BOARD OF EXAMINERS

_____

_____

(SIGNATURE OF EXAMINERS)

*Only in case the thesis is approved

Declaration of Originality and Compliance of Academic Ethics

I hereby declare that this thesis contains literature survey and original research work by the undersigned candidate, as part of his **Master of Electrical Engineering** studies.

All information in this document have been obtained and presented in accordance with academic rules and ethical conduct.

I also declare that, as required by these rules and conduct, I have fully cited and referenced all materials and results that are not original to this work.

NAME:	**SHRAMANA GUHA SARKAR**
REGISTRATION NO.:	128909 of 2014-15
ROLL NO.:	M4ELE16-16
THESIS TITLE:	**Studies on Some Brain MRI Segmentation Techniques Suitable for Online Applications**

DATE :

PLACE: KOLKATA

_____

(SHRAMANA GUHA SARKAR)

ACKNOWLEDGEMENTS

I would like to take this opportunity to humbly express my gratitude for the innumerable gestures of help, co-operation and inspiration that I have received from my teachers, friends and well-wishers during my post graduate course.

I feel honoured to express my profound regard and deep sense of gratitude to my guides Dr. Debangshu Dey and Prof. Biswajit Bhattacharyya, Department of Electrical Engineering, Jadavpur University, Kolkata, for allowing me to do my work in this exciting field. I am highly obliged and grateful for their excellent guidance, endless encouragement, continuous motivation and unique cooperation extended to me, right from the very beginning of onset of this task till its successful completion.

I am also sincerely grateful to Dr. A. Chatterjee, Prof. S. Munshi, Prof. P. K. Kundu, Prof. M. Dutta and Dr. G. Sarkar for their keen interest and active support in this work.

I would like to thank Prof. Swapan Kumar Goswami, Head of the Department of Electrical Engineering for providing me with necessary facilities for carrying out this thesis work.

I am thankful to my friends Debabrata Mahis, Subhabrata Naskar, Joy Banerjee, Nabanita Chatterjee, Pitar Mandal and to PhD research scholars Saptarshi Chatterjee and Sayanti Chaudhuri for providing valuable suggestions and making our lab such a great and memorable place to work.

Finally, I gratefully acknowledge the constant support, love and encouragement of my parents without whom nothing would have been possible.

Date: _____

Place: Jadavpur University, Kolkata. (SHRAMANA GUHA SARKAR)

TABLE OF CONTENTS

CHAPTER-1 INTRODUCTION (1)

CHAPTER-2 MATHEMATICAL MORPHOLOGY AIDED SEGMENTATION OF BRAIN MRI USING FUZZY C-MEANS CLUSTERING

2.1 Introduction (7)

2.2 Overview of Mathematical Morphology (9)

2.2.1 Basic mathematical background (9)

2.2.2 Dilation (10)

2.2.3 Erosion (11)

2.2.4 Opening (12)

2.2.5 Closing (13)

2.2.6 Morphological top hat filters (14)

2.3 Proposed Scheme of Work (15)

2.3.1 Pre-processing (16)

2.3.2 Image Enhancement by mathematical morphology (18)

2.3.3 Segmentation of brain tissues using (19)

FCM

2.4 Results and Discussions (21)

2.4.1 Dataset Description and Parameter Setting (21)

2.4.2 Qualitative Evaluation (21)

2.4.3 Quantitative Evaluation (23)

2.5 Conclusions (28)

References (30)

CHAPTER-3 MULTILEVEL OPTIMAL THRESHOLDING OF BRAIN MRI USING A MODIFIED HYBRIDIZED BAT ALGORITHM (MHBA)

3.1 Introduction (34)

3.2 Entropy based multilevel image thresholding (36)

3.2.1 Overview (36)

3.2.2 Fuzzy entropy based multilevel image Thresholding (37)

3.3 Basic Bat Algorithm (BA) adapted for multilevel image thresholding (42)

3.3.1 Echolocation behaviour of micro bats (42)

3.3.2 Assumptions (42)

3.3.3 The Bat Algorithm (BA) (43)

3.3.4 Pseudocode of BA (45)

3.4 Proposed Modified Hybridized Bat Algorithm (MHBA) for multilevel image thresholding (47)

3.4.1 Background behind improvement of BA (47)

3.4.2 Doppler Effect in MHBA (47)

3.4.3 Crossover, Mutation and Scout technique in MHBA (48)

3.4.4 Proposed MHBA (49)

3.4.5 Pseudocode of MHBA (52)

3.5 Results and Discussions (54)

3.5.1 Parameter Setting (54)

3.5.2 Qualitative and Quantitative Analysis (55)

3.6 Conclusions (64)

References (66)

CHAPTER-4 MICROCONTROLLER BASED COMMUNICATION SYSTEM FOR APPLICATIONS IN TELEHEALTH

4.1 Introduction (71)

4.2 Overview of the present scheme (72)

4.3 Hardware and its overview (73)

4.4 Software Implementation (75)

4.5 Experimental Results (76)

4.6 Conclusions (79)

CHAPTER-5 CONCLUSIONS AND FUTURE WORK

5.1 Conclusions (80)

5.2 Future Work (81)

CHAPTER 1

INTRODUCTION

Medical imaging is the technology and process of creating visual representations of the interior of a body for clinical analysis and medical intervention, as well as visual representation of the function of some organs or tissues. The purpose of medical imaging is to reveal internal structures hidden by the skin and bones, as well as to diagnose and treat disease. It also establishes a database of normal anatomy and physiology to make it possible to identify abnormalities. [13]

Over the last few decades, the rapid development of noninvasive brain imaging technologies has opened new horizons in analyzing and studying the brain anatomy and function. Enormous progress in accessing brain injury and exploring brain anatomy has been made using magnetic resonance imaging (MRI) [1]. The ability of MRI to produce high resolution spatial images and its sensitivity towards differentiating neurological tissues helps in diagnosis, prognosis, pre-surgical and post-surgical treatment planning for various diseases, e.g., multiple sclerosis, Parkinson's disease, epilepsy, cerebral atrophy, Alzheimer's disease etc. [5].

Brain MRI segmentation is thus a crucial task because it influences the outcome of the entire analysis since different processing steps rely on accurate segmentation of anatomical regions. For example, MRI segmentation is commonly used for measuring and visualizing different brain structures, for delineating lesions, for analyzing brain development, and for image guided interventions and surgical planning.

Until recently, manual tracing of brain regions by experts in neuro-anatomy has been the accepted standard. However, there are quite a few limitations of manual segmentation. As the size of the MRI datasets has increased, the time and cost required for the labor intensive process of manual tracing has become unaffordable. An experienced researcher may require a few hours to trace a single structure, and more than a week to trace all of the major structures of the brain [2]. Moreover, differences in criteria among experts can lead to methodically different volume estimates of some brain regions. So the highest consistency and sensitivity is achieved when a

single individual traces the entire dataset. However, time becomes a major constraint in this aspect and also the criteria used by even a trained expert can subtly drift during the course of a long study. For these reasons, automated procedures for segmenting and quantifying the brain have attracted considerable interest and has led to development of various segmentation techniques of different accuracy and degree of complexity. These automated methods provide consistent results with repeated iterations on a given dataset. Improvements in the segmentation algorithms can be accommodated with relative ease even on large data sets by re-analysis with updated software [2]. The automated segmentation methods, with application to brain MRI, may be grouped as follows:

(1) intensity-based methods (including thresholding, region growing, classification, and clustering);
(2) atlas-based methods;
(3) surface-based methods (including active contours and surfaces, and multiphase active contours);
(4) hybrid segmentation methods

Over the years, many researchers have proposed various segmentation techniques that are widely being used. One of the earliest works in this domain include 3-D reconstruction of the brain from anisotropic MRI brain data [9]. The scheme encompasses an automatic segmentation technique that includes a gray level thresholding of white matter and gray matter, a global white matter segmentation with 3-D connectivity and gray matter segmentation with a local 3-D connectivity. Expectation/Maximization (EM) segmentation, binary mathematical morphology and active contour models have been utilized in [3] for brain MRI segmentation. Each of these techniques has been customized for the problem of brain tissue segmentation such that the resultant method is more robust than its components. A fully automatic segmentation of brain MRI employing anisotropic filters, 'snakes' contouring techniques and *a priori* knowledge has been proposed in [12]. It is a multistage process, involving removal of the background noise leaving a head mask, then finding a rough outline of the brain, then refinement of the rough brain outline to a final mask. A constrained Gaussian mixture model framework for automated tissue segmentation of noisy, low-contrast MR images of the brain is presented in [8]. The intensity of a tissue is considered a global feature and is incorporated into the model through tying of all the related Gaussian parameters. The expectation-maximization (EM) algorithm is utilized to learn the parameter-tied,

constrained Gaussian mixture model. An elaborate initialization scheme is suggested to link the set of Gaussians per tissue type, such that each Gaussian in the set has similar intensity characteristics with minimal overlapping spatial supports. A framework that combines atlas registration, fuzzy connectedness (FC) segmentation, and parametric bias field correction (PABIC) has been proposed in [10] for the purpose of automated brain MRI segmentation. Original techniques are proposed to estimate necessary initial parameters of FC segmentation. Further, the result of the FC segmentation is utilized to initialize a following PABIC algorithm. Finally, the FC technique has been re-applied on the PABIC corrected MRI to get the final segmentation. In [5], a novel, optimal multilevel thresholding algorithm called BACTFOR has been proposed for automatic brain MRI segmentation. The work in [5] is especially suitable for multimodal image histograms, for segmentation of T2 weighted brain MRI. In [11], an adaptive mean-shift methodology has been utilized to segment the MRI brain voxels into its constituent tissues. In this work, the MRI image space has been represented by a high-dimensional feature space that includes multimodal intensity features as well as spatial features. An adaptive mean-shift algorithm clusters the joint spatial-intensity feature space, thus extracting a representative set of high-density points within the feature space, otherwise known as modes. Tissue segmentation is obtained by a follow-up phase of intensity-based mode clustering into the three tissue categories. Particle swarm optimization (PSO) aided level set based global fitting energy active contour approach has been employed in [4] for robust medical image segmentation including brain MRI. In this work, a robust version of the Chan and Vese algorithm which is expected to achieve satisfactory segmentation performance, irrespective of the initial choice of contour has been utilized. For the purpose of automated brain MRI segmentation, a conditional spatial fuzzy C-means clustering algorithm has been proposed in [6] to improve the robustness of the conventional FCM. In this work, the problem of sensitivity to noise and intensity inhomogeneity in MRI data is efficiently reduced by incorporating local and global spatial information into a weighted membership function. In [7], supervised classification has been employed for automatic segmentation of MR brain images of preterm infants. The algorithm uses supervised voxel classification in three subsequent stages for tissue labelling, dedicated analysis and multi-class classification respectively.

This thesis work, presents two comparatively new, unsupervised brain MRI segmentation schemes based on clustering and thresholding methods. In the first scheme, a novel mathematical morphology aided image enhancement technique has been utilized and a better clustering performance has been obtained upon application of FCM. In the second scheme, a comparatively recent metaheuristic algorithm called the Bat Algorithm (BA) has been applied to obtain a thresholding based brain MRI segmentation and in order to improve the performance, a successful modification to the basic BA to form a Modified Hybridized Bat Algorithm (MHBA) has been carried out. Moreover, for telehealth applications, a microcontroller based communication system has been developed which utilizes the existing LAN setup of a distributed system like a hospital or a diagnostic center. It acts as a dedicated *store-and-forward* system also having the provision for real-time data transfer and it can be used to transmit the data points corresponding to the segmented regions of the brain MRI as and when required to an off-site medical practitioner.

The thesis is organized as follows:

- Chapter 2 presents a mathematical morphology aided novel brain T2 MR image enhancement technique followed by clustering using Fuzzy C-means clustering (FCM) algorithm.
- Chapter 3 proposes a novel Modified Hybridized Bat Algorithm (MHBA) for multilevel thresholding of brain MRI and compares the segmentation results with those obtained from using the basic Bat Algorithm (BA).
- Chapter 4 explains the proposed microcontroller based communication scheme for telehealth applications.
- Chapter 5 concludes the thesis along with a discussion for future scope of work.

References

[1] Ivana Despotović, Bart Goossens and Wilfried Philips. "MRI Segmentation of the Human Brain: Challenges, Methods, and Applications". Computational and Mathematical Methods in Medicine, Vol. 2015, Article ID 450341, 23 pages.

[2] Rajendra A. Morey, Christopher M. Pettya, Yuan Xu, Jasmeet Pannu Hayes, H. Ryan Wagner II, Darrell V. Lewis, , Kevin S. LaBar, Martin Stynerg,h, and Gregory McCarthy. "A Comparison of Automated Segmentation and Manual Tracing for Quantifying Hippocampal and Amygdala Volumes". Neuroimage, 2009 April 15; 45(3): 855-866.

[3] Tina Kapur, W. Eric L. Grimson, William M. Wells III and Ron Kikinis. "Segmentation of Brain Tissue from Magnetic Resonance Images". Medical Image Analysis (1996) Vol. 1, no. 2, pp 109-127.

[4] Devraj Mandal, Amitava Chatterjee and Madhubanti Maitra. "Robust Medical Image Segmentation using Particle Swarm Optimization Aided Level Set Based Global Fitting Energy Active Contour Approach". Engineering Applications of Artificial Intelligence 35 (2014), 199-214.

[5] Madhubanti Maitra and Amitava Chatterjee. "A Novel Technique for Multilevel Optimal Magnetic Resonance Brain Image Thresholding using Bacterial Foraging". Measurement 41 (2008), 1124-1134.

[6] Sudip Kumar Adhikari, Jamuna Kanta Sing, Dipak Kumar Basu and Mita Nasipuri. "Conditional Spatial Fuzzy C-Means Clustering Algorithm for Segmentation of MRI Images". Applied Soft Computing 34 (2015), 758-769.

[7] Pim Moeskops, Manon J.N.L. Benders, Sabina M. Chiţă, Karina J. Kersbergen, Floris Groenendaal, Linda S. de Vries, Max A. Viergever and Ivana Išgum. "Automatic Segmentation of MR Brain Images of Preterm Infants using Supervised Classification". NeuroImage 118 (2015), 628-641.

[8] Hayit Greenspan, Amit Ruf and Jacob Goldberger. "Constrained Gaussian Mixture Model Framework for Automatic Segmentation of MR Brain Images". IEEE Trans. on Medical Imaging, Vol. 25, no. 9, September, 2006, pp.1233-1245.

[9] Marc Joliot and Bernard M. Mazoyer. "Three-Dimensional Segmentation and Interpolation of Magnetic Resonance Brain Images". IEEE Trans. on Medical Imaging, Vol. 12, no. 2, June, 1993, pp.269-277.

[10] Yongxin Zhou and Jing Bai. "Atlas-Based Fuzzy Connectedness Segmentation and Intensity Nonuniformity Correction Applied to Brain MRI". IEEE Trans. on Biomedical Engineering, Vol. 54, no. 1, January, 2007, pp.122-129.

[11] Arnaldo Mayer and Hayit Greenspan. "An Adaptive Mean-Shift Framework for MRI Brain Segmentation". IEEE Trans. on Medical Imaging, Vol. 28, no. 8, August, 2009, pp.1238-1250.

[12] M. Stella Atkins and Blair T. Mackiewich. "Fully Automatic Segmentation of the Brain in MRI". IEEE Trans. on Medical Imaging, Vol. 17, no. 1, February, 1998, pp.98-107.

[13] https://en.wikipedia.org/

CHAPTER 2

MATHEMATICAL MORPHOLOGY AIDED SEGMENTATION OF BRAIN MRI USING FUZZY C-MEANS CLUSTERING

2.1 Introduction

The term 'morphology' means the study of shape, form or structure of objects. Mathematical morphology deals with the mathematical theory of describing shapes using set theory, integral geometry and lattice algebra. It was developed in 1964 by the collaborative work of Georges Matheron and Jean Serra. Appropriately used, morphological operators tend to simplify image processing by preserving the essential shape characteristics and eliminating irrelevant features [2]. Mathematical morphology based image processing has gained immense popularity in the recent past and there still remains a lot to be explored. The scope of mathematical morphology in image processing spans image enhancement, image segmentation, image measurements, texture analysis etc. and it has found its use in various areas of image processing applications.

Pesaresi *et al.* [4] proposed a novel method of high resolution satellite imagery segmentation based on the mathematical morphology based characteristic of connected components in images. The proposed method used the residuals of morphological opening and closing transforms based on geodesic metric. Valero *et al.* [16] used directional mathematical morphology based operators for detection of road networks in very high resolution remote sensing images. In order to extract structural pixel information, the authors used Path Openings and Path Closings. Pan *et al.* [6] proposed a novel method of segmentation of pores in wood microscopic images based on mathematical morphology employing a variable structuring element and also by adaptive thresholding. Landström *et al*. [7] developed an automated on-line crack detection system for steel slabs based on 3D profile data of steel slab surfaces utilizing morphological image processing techniques and statistical classification by logistic regression. Serna *et al*. [10] used mathematical morphology and supervised learning for detection, segmentation and classification of 3D urban objects. Liu *et al.* [12] proposed a novel binarization method for strip steel defect image with non-uniform illumination based on mathematical morphology and genetic algorithm. The proposed method in [12] constituted an enhancement operator based on mathematical morphology and the

experimental results have shown that the proposed method outperforms the traditional image binarization methods. In [22], mathematical morphology has been applied to sensor network applications. The images have been compressed using the quad tree data structure and also processed in this structure using morphological operations to achieve the sensing purpose. Jimeno-Morenilla *et al.* [28] proposed a design and manufacturing model based on set theory and mathematical morphology. Yu *et al.* [24] developed a novel shape representation algorithm based on mathematical morphology and the algorithm proved to be immune to noise and occlusion and invariant under rotation, translation and scaling.

Moreover, in recent times mathematical morphology has found numerous applications in state-of-the-art biomedical image processing techniques. Said *et al.* [21] used mathematical morphology for teeth segmentation in digitized dental x-ray films. Naegel [25] proposed a novel scheme for labeling of vertebrae from 3D CT-scan images employing mathematical morphology. Halkiotis *et al.* [26] utilized mathematical morphology along with neural networks for automatically detecting clustered microcalcifications in digital mammograms. In this method, morphological filters have been applied to remove noise and regional maxima that do not correspond to calcifications. A novel fovea center detection based on the retina anatomy and mathematical morphology was proposed by Welfer *et al.* [29]. Luengo-Oroz *et al.* [5] employed morphological techniques for robust iris segmentation on uncalibrated noisy images. Bouraoui *et al.* [19] have used mathematical morphology concepts of grey-level-hit-or-miss transform for the design of an automatic method for segmenting coronary arteries in large 3D CTA (computed tomography angiography). Hassan *et al.* [20] and Sigurðsson *et al.* [18] respectively employed mathematical morphology for retinal blood vessel segmentation. Mathematical morphology has also been implemented for bone marrow biopsy segmentation in [23]. Dufour *et al.* [30] used mathematical morphology vessel segmentation and filtering of 3D angiographic data.

Mathematical morphology has also found quite a few applications in brain MRI processing. Stokking *et al.* [13] merged morphological operators like erosion and geodesic dilation along with thresholding and region growing techniques for fully automatic brain extraction from MRI-T1 data. Gui *et al.* [8] proposed a more elaborate and detailed method where MR images of the neonatal brain were segmented both globally (intracranial cavity, cerebellum, brainstem and the two hemispheres) and at tissue level (cortical and subcortical gray matter, myelinated and unmyelinated white matter, and cerebrospinal fluid) using morphological operators aided by

region growing and watershed transform. Our present work in this chapter focuses on utilizing mathematical morphology based operators for developing a novel and simple pre-processing and image enhancement technique resulting in efficient segmentation of human brain MRI-T2 images into three regions- white matter (WM), gray matter (GM) and cerebrospinal fluid (CSF). The enhanced MRI-T2 images are segmented using fuzzy C-means (FCM) clustering method. Fuzzy segmentation methods, especially FCM algorithms have found a wide use in brain MRI segmentation because in comparison to hard segmentation methods they retain much more information and result in more efficient segmentation of brain tissues [31-36].

The rest of the chapter is organized as follows. In Section 2.2 an overview of mathematical morphology is presented. Section 2.3 deals with elaborately discussing the scheme of the proposed work. The basics of the FCM algorithm is also discussed in this section. Section 2.4 contains the detailed experimental results and discussions. The chapter is concluded in Section 2.5.

2.2 Overview of Mathematical Morphology

2.2.1 Basic mathematical background:

Mathematical morphology acts as an effective method for extracting specific shapes and structures of interest from a binary or gray-scale digital image. The basic tools are the morphological operations *dilation* and *erosion*. A morphological operator transforms an image by means of a *structuring element* (which is chosen by the user) into a new image. A structuring element is nothing but a small set used to probe the image thereby highlighting the structures having similar shape. [1].

Mathematical morphology can be applied to a finite set P if [43]

1. Its elements can be *partially ordered* (where the ordering is denoted by "$\leq$" which has its usual meaning) i.e., for all a, b, c$\in$P

$$a \leq a$$

$$(a \leq b, b \leq a) \Rightarrow a = b$$

$$(a \leq b, b \leq c) \Rightarrow a \leq c$$

and

2. Each non-empty subset of P has a maximum and minimum. (The maximum and minimum are also defined in the usual sense).

This concept of partial ordering can further be extended to digital images by applying the rules to the individual pixels. For instance, for two images *f* and *g* the relation $f \leq g$ holds if:

$$f \leq g \;\Leftrightarrow\; \forall x: \big(f(x) \leq g(x)\big),$$

where "$\forall x$" refers to all possible pixel locations. The "maximum image" and "minimum image" of two images can also be defined on a pixel-wise basis:

$$(\max\{f, g\})(x) = \max\{f(x), g(x)\}$$
$$(\min\{f, g\})(x) = \min\{f(x), g(x)\}$$

The concepts of ordering, maximum and minimum are fundamental in mathematical morphology. The basic morphological operations are discussed as follows.

2.2.1 Dilation:

The dilation of a set (binary image) X by a structuring element B is denoted by $\delta_B(X)$ and is defined as the locus of points x such that B hits X when its origin coincides with x [1]:

$$\delta_B(X) = \{x | B_x \cap X \neq \emptyset\}. \qquad (2.1)$$

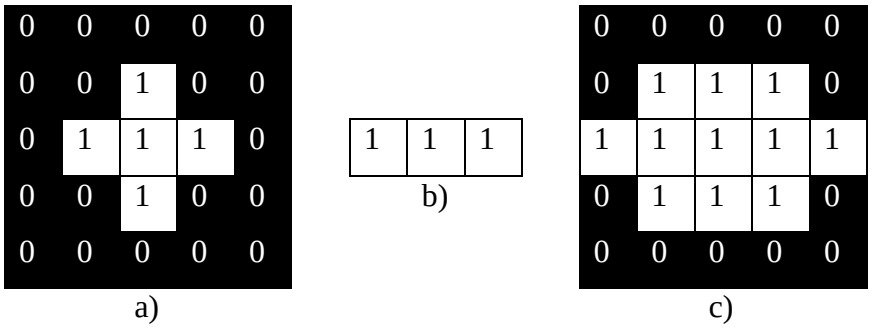

Fig 2.1 shows a simple 5x5 binary image X (a). White pixels have intensity 1 and black pixels have intensity 0. A 1x3 simple structuring element B (b). The resultant image after dilation operation (c).

The dilation by a symmetrical structuring element is described more intuitively by [43]:

- Place the structuring element anywhere in the image.

- Does it hit the set? Then origin of the structuring element is a part of the dilated image.

In case of gray level images, dilation is defined as: The dilated value at a given pixel x is the maximum of the image *f* in the window defined by the structuring element when its origin is at x [1]:

$$[\delta_B(f)](x) = max_{b \in B}\, f(x+b) \qquad (2.2)$$

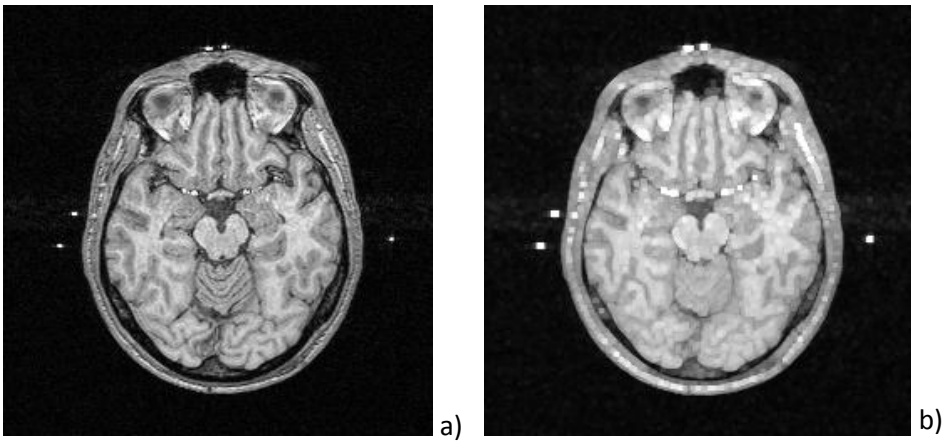

Fig 2.2 Original gray scale image (a). Example of dilation by a 3x3 square structuring element (b).

2.2.3 Erosion

The erosion of a set (binary image) X by a structuring element B is denoted by $\varepsilon_B(X)$ and is defined as the locus of points x such that B is included in X when its origin coincides with x [1]:

$$\varepsilon_B(X) = \{x | B_x \subseteq X\}. \qquad (2.3)$$

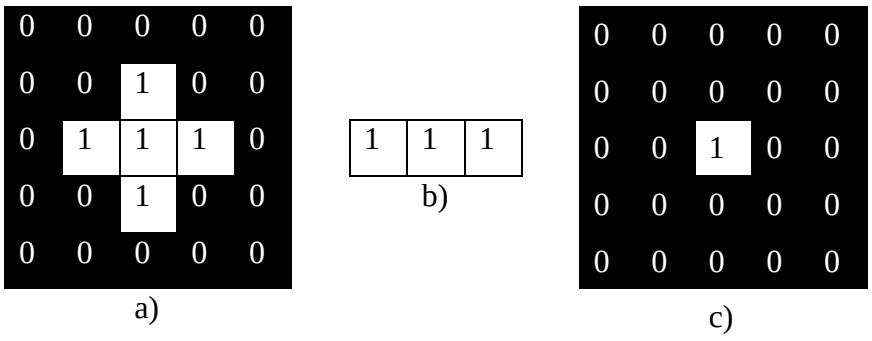

Fig 2.3 shows a simple 5x5 binary image X (a). White pixels have intensity 1 and black pixels have intensity 0. A 1x3 simple structuring element B (b). The resultant image after erosion operation (c).

The erosion by a symmetrical structuring element is described more intuitively by [43]:

- Place the structuring element anywhere in the image
- Is it fully contained by the set (i.e., a subset)? Then the origin of the structuring element is part of the eroded set.

In case of gray scale image, the definition of erosion is given by: The eroded value at a given pixel x is the minimum value of the image *f* in the window defined by the structuring element when its origin is at x [1]:

$$[\varepsilon_B(f)](x) = min_{b\in B} f(x + B). \quad (2.4)$$

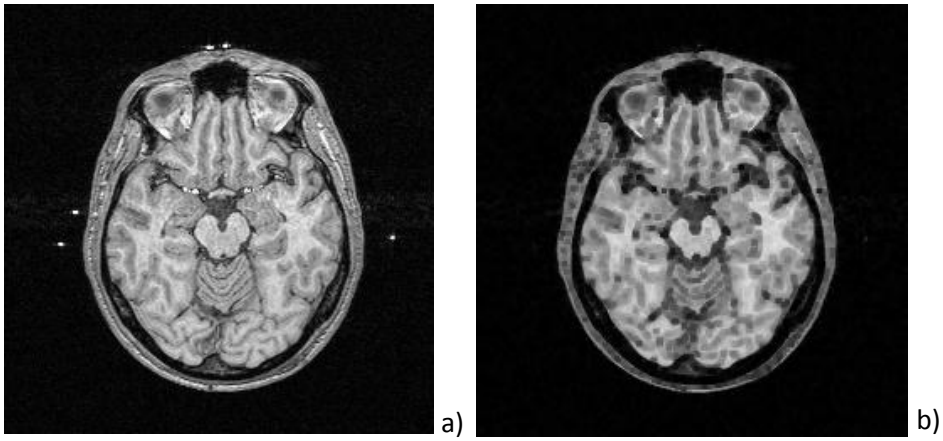

Fig 2.4 Original gray scale image (a). Example of erosion by a 3x3 square structuring element (b).

2.2.4 Opening

The opening γ of an image *f* by a structuring element B is denoted by $\gamma_B(f)$ and is defined as the erosion of *f* by *B* followed by the dilation with the reflected structuring element (SE) B' [1]*:*

$$\gamma_B(f) = \delta_{B'}[\varepsilon_B(f)], \quad (2.5)$$

It can be further explained as [43]:

"Does the structuring element fit the set?" Each time the answer to this question is affirmative, the *whole* SE must be kept (for the erosion, it is the origin of the SE that is kept).

Therefore, the opened set is the union of all SEs fitting the set:

$$\gamma_B(X) = \cup_x\{B_x | B_x \subseteq X\}. \quad (2.6)$$

Once an image has been eroded, there exists in general no inverse transformation to get the original image back. The idea behind the morphological opening is to dilate the eroded image to recover as much as possible the original image.

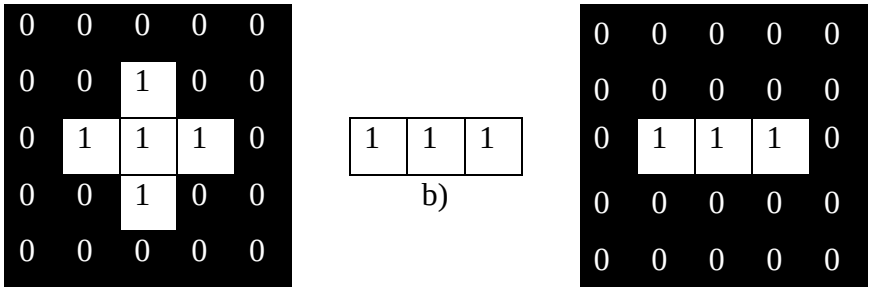

Fig 2.5 shows a simple 5x5 binary image X (a). White pixels have intensity 1 and black pixels have intensity 0. A 1x3 simple structuring element B (b). The resultant image after opening operation (c).

2.2.5 Closing:

The closing ϕ of an image *f* by a structuring element B is denoted by $\phi_B(f)$ and is defined as the dilation of *f* by *B* followed by the erosion with the reflected structuring element (SE) B' [1]*:*

$$\emptyset_B(f) = \varepsilon_{B'}[\delta_B(f)], \quad (2.6)$$

Another definition [43]:

"Does the structuring element fit the background of the set?". Each time the answer is affirmative, all points of the structuring element belong to the complement of the closing set:

$$\emptyset_B(X) = [\cup_x\{B_x | B_x \subseteq X^c\}]^c. \quad (2.7)$$

The idea behind the morphological closing is to build an operator tending to recover the initial shape of the image structures that have been dilated. This is achieved by eroding the dilated image.

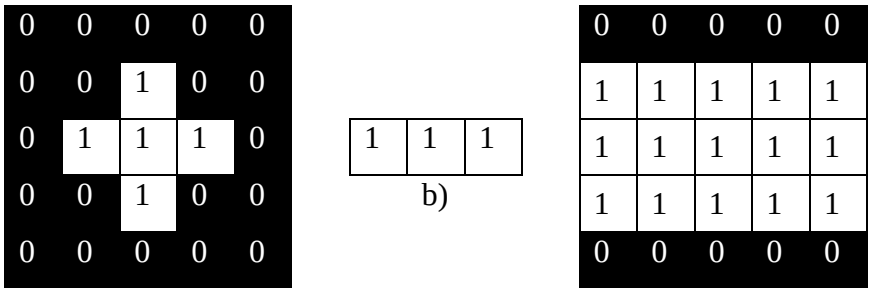

Fig 2.6 shows a simple 5x5 binary image X (a). White pixels have intensity 1 and black pixels have intensity 0. A 1x3 simple structuring element B (b). The resultant image after closing operation (c).

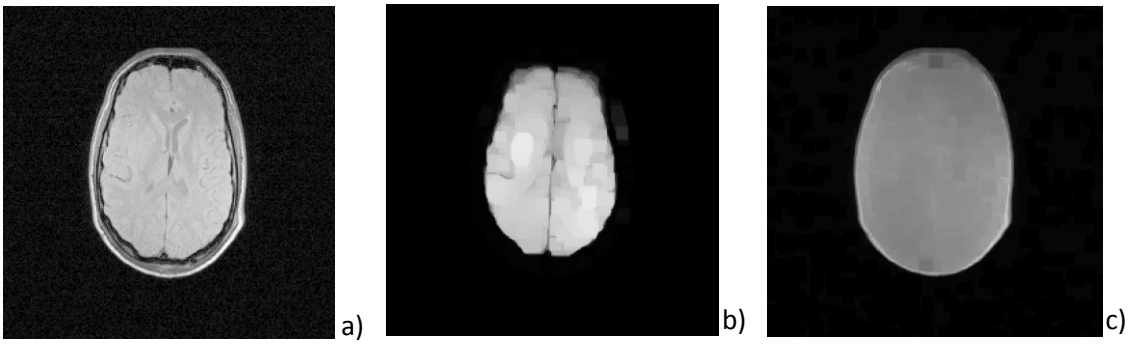

Fig 2.7 Example of opening (b) and closing (c) by a square structuring element on a grey valued MR image (a).

2.2.5 Morphological top hat filters:

An opening can be used to remove structures smaller than a certain size from an image, while not –or rather, as little as possible–altering larger structures. The closing operation can be used to close up holes and cavities that are smaller than a certain size. If an opening removes small structures, then the difference of the original image and the opened image should bring them out. This is exactly what the *white top hat T*(*f*) filter does, which is defined as the residue of the original and opening [1,43]:

$$T(f) = f - \gamma(f). \qquad (2.8)$$

The top hat filter brings out or highlights small bright structures of the image that are smaller in size and similar in shape to the structuring element. Another important feature of the top hat filter is that not only does it show small structures, but it shows them with a grey value that is *relative to the local background:* the grey value of the extracted small structures is relative to the local

grey value in the neighborhood in the original image. In this way, slow grey value variations in the background of an image, *e.g.*, an illumination gradient in a photograph can be removed [43].

The counterpart of the white top hat is the *black top hat filter* $T^*(f)$ which is defined by the residue of closed image and original image [1,43]:

$$T^*(f) = \emptyset(f) - f. \tag{2.9}$$

As the white top hat extracts small "white" structures (larger grey value than the background), the black top hat extracts small "dark" structures, *i.e.*, holes and cavities. The shape size and orientation of the structuring element used for top hat filtration completely depends on the morphology of the image artifacts that are wished to be extracted.

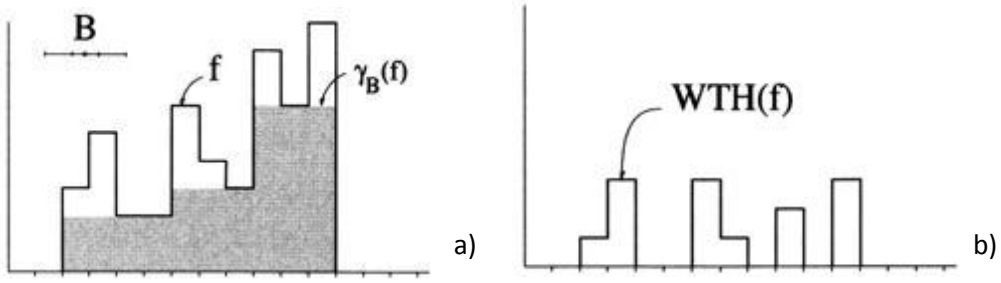

Fig 2.8 Original image *f* and its opening γ by B (a). Image after applying white top hat filter (b).

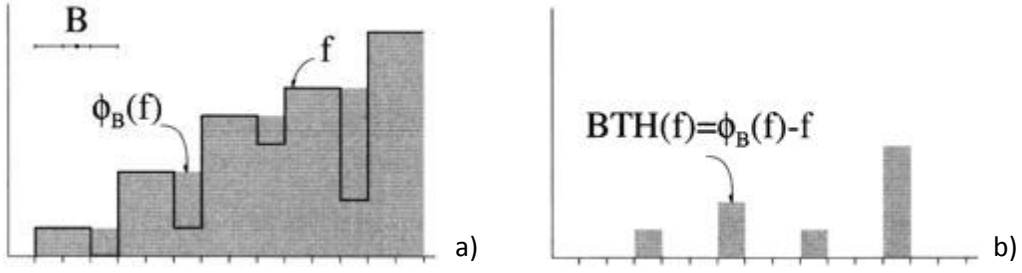

Fig 2.9 Original image *f* and its closing ϕ by B (a). Image after applying black top hat filter (b).

2.3 Proposed scheme of work

The methodology of our proposed work can be represented very simply by the following block diagram:

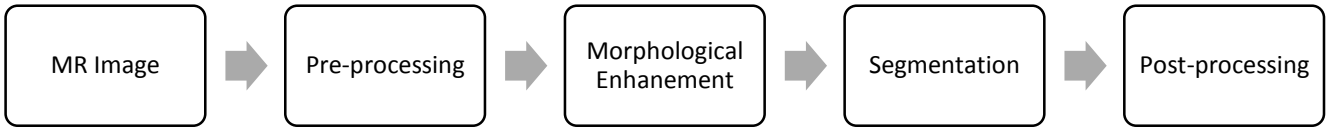

Fig 2.10 Block Diagram of proposed methodology

2.3.1 Pre-processing:

MR images are obtained based on the principle that whenever protons are exposed to electromagnetic radiation they absorb energy and after some time, to return to their equilibrium stage the nuclei reradiate this energy which is observed as the MR image. MR images are mostly corrupted by two irregularities- one is the intensity inhomogeneity which is nothing but the low frequency spatially varying artifact causing a smooth signal intensity variation within tissue of the same physical properties, and the other is a noise following Gaussian distribution [37]. The presence of these irregularities highly reduces the tissue segmentation performance and thus have to be removed. In our work a simple method for noise removal has been proposed which takes the aid of mathematical morphology and other conventional filters. The pre-processing steps are:

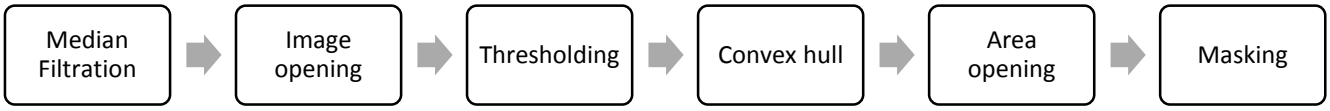

Fig 2.11 Block diagram of pre-processing steps.

For the removal of Gaussian noise, a 3x3 median filter has been used. Then, to improve the output of the median filter, a *morphological opening* operator is used with a very small circular structuring element to remove the remaining maximum values that are smaller than the structuring element [18]. Next, in order to remove the other irrelevant image artifacts and extract the brain, Otsu's thresholding is performed, after that the convex hull of the binary image is extracted, the maximum area of foreground objects is calculated and an area opening is performed to produce

the final mask which extracts the brain from its surroundings. The entire pre-processing steps are shown in Fig 2.12.

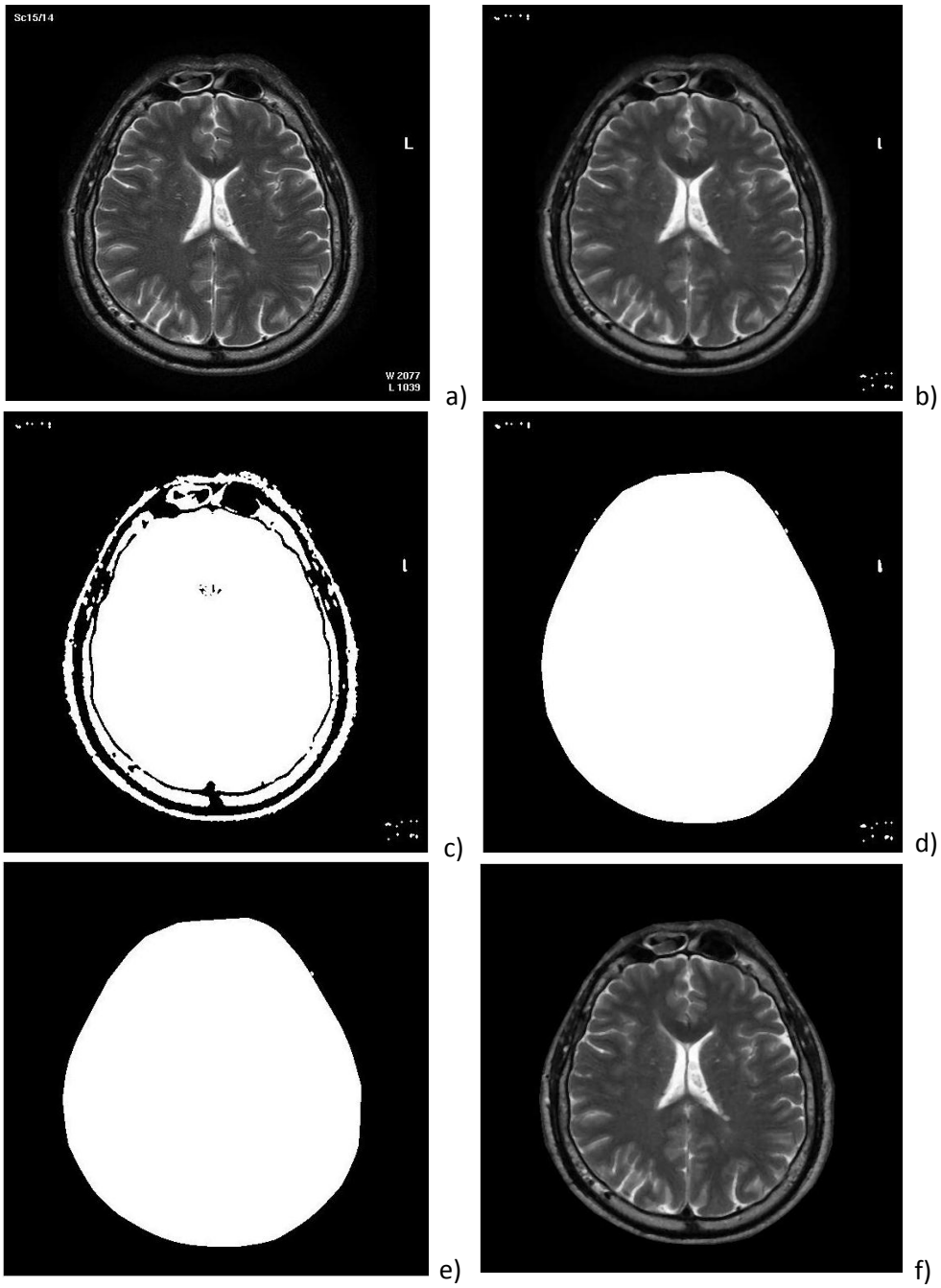

Fig 2.12 Pre-processing steps: (a) original image, (b) image after median filtration and opening, (c) image after thresholding using Otsu's method, (d) convex hull image, (e) maximum area image after area opening, (f) final processed image after masking (a) with (e).

2.3.2 Image Enhancement by Mathematical Morphology:

Morphological *top hat filters* are applied on the processed MR image. In order to get effective results from a morphological operation, choosing an appropriate structuring element is very important. Line and circular structuring elements are chosen since they correspond to the structures of the lateral ventricles and the CSF filled furrows of the brain. There will not be any change with the line-like CSF structures if the structuring elements are parallel with these brain structures [20]. So, the best response has been obtained by applying linear structuring elements to the digital image at various directions. The line structuring element are applied in 4 directions: 0^o, 45^o,90^o and 135^o. Then the computational results have been summed up at these 4 directions. Thus the gray differences between the CSF structures and the background are increased [20]. The resultant image is then morphologically *closed* by a circular SE.

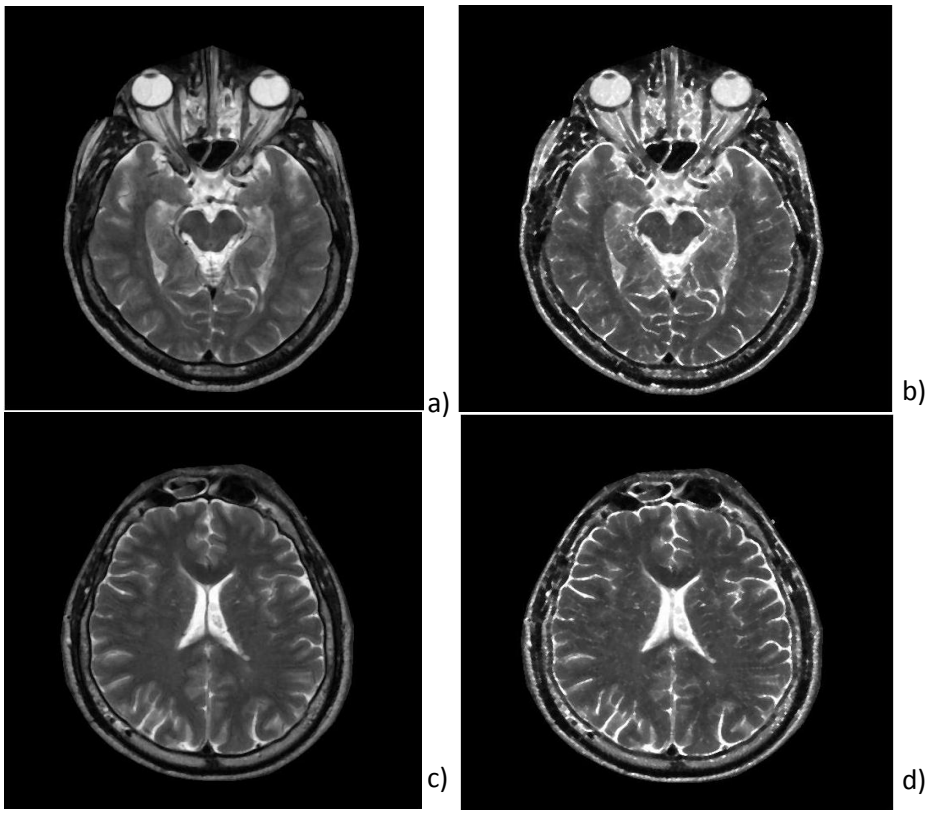

Fig 2.13 (a), (c): original MR images, (b), (d): corresponding morphologically enhanced MR images

2.3.3 Segmentation of brain tissues using FCM:

Fuzzy C-means clustering is employed for segmenting the brain MRI tissues into three clusters- WM, GM and CSF. The FCM clustering algorithm proposed by Dunn and improved by Bezdek, is an improvement of the hard k-means algorithm [34]. FCM is a fuzzy clustering method based on the minimization of a quadratic criterion where clusters are represented by their respective centers. It assigns a class membership to a data point, depending on the similarity of the data point to a particular class relative to all other classes. The standard FCM objective function of partitioning an image into *c* clusters is given by:

$$J_m(\mu, v) = \sum_{i=1}^{c} \sum_{j=1}^{n} \mu_{ij}^{m} d^2(x_j, v_i) \quad (2.10)$$

subject to $\sum_{i=1}^{c} \mu_{ij} = 1$ (2.11)

Where $X=(x_1,x_2,\ldots,x_j,\ldots,x_n)$ is a data matrix of size pxn, p represents the dimension of each x_j "feature" vectors (pixel numbers in the image). The feature vector X in MR images is the pixel intensity, so p=1. μ_{ij} is the membership of the j^{th} data in i^{th} cluster c_i, m presents the index of fuzziness (in this study, m=2), and v_i is the fuzzy cluster centroid of the i^{th} cluster. Using the Euclidean norm, the distance metric d measures the similarity between a feature vector x_j and a cluster centroid v_i in the feature space i.e.,

$$d^2(x_j, v_i) = \left||x_j - v_i\right||^2 \quad (2.12)$$

||.|| is any norm expressing the similarity measure.

Typically, the Euclidean distance measure is used. The objective function is minimized when the large membership values are assigned to input patterns that are close to their nearest cluster centers and low membership values are assigned when they are far from the cluster centers. Minimizing the objective function with the given constrain (2.11), the following equations are obtained.

$$\frac{\partial J_m}{\partial \mu_{ij}} = 0, and\ \frac{\partial J_m}{\partial v_i} = 0. \quad (2.13)$$

These lead to the following iterative solutions:

$$\mu_{ij} = \frac{1}{||x_j - v_i||^{\frac{2}{m-1}} \Big/ \sum_{i=1}^{c} ||x_j - v_i||^{\frac{2}{m-1}}} \quad (2.14)$$

And

$$v_i = \frac{\sum_{j=1}^{n} \mu_{ij}^m x_k}{\sum_{j=1}^{n} \mu_{ik}^m} \quad (2.15)$$

The flowchart of the FCM algorithm is given as follows:

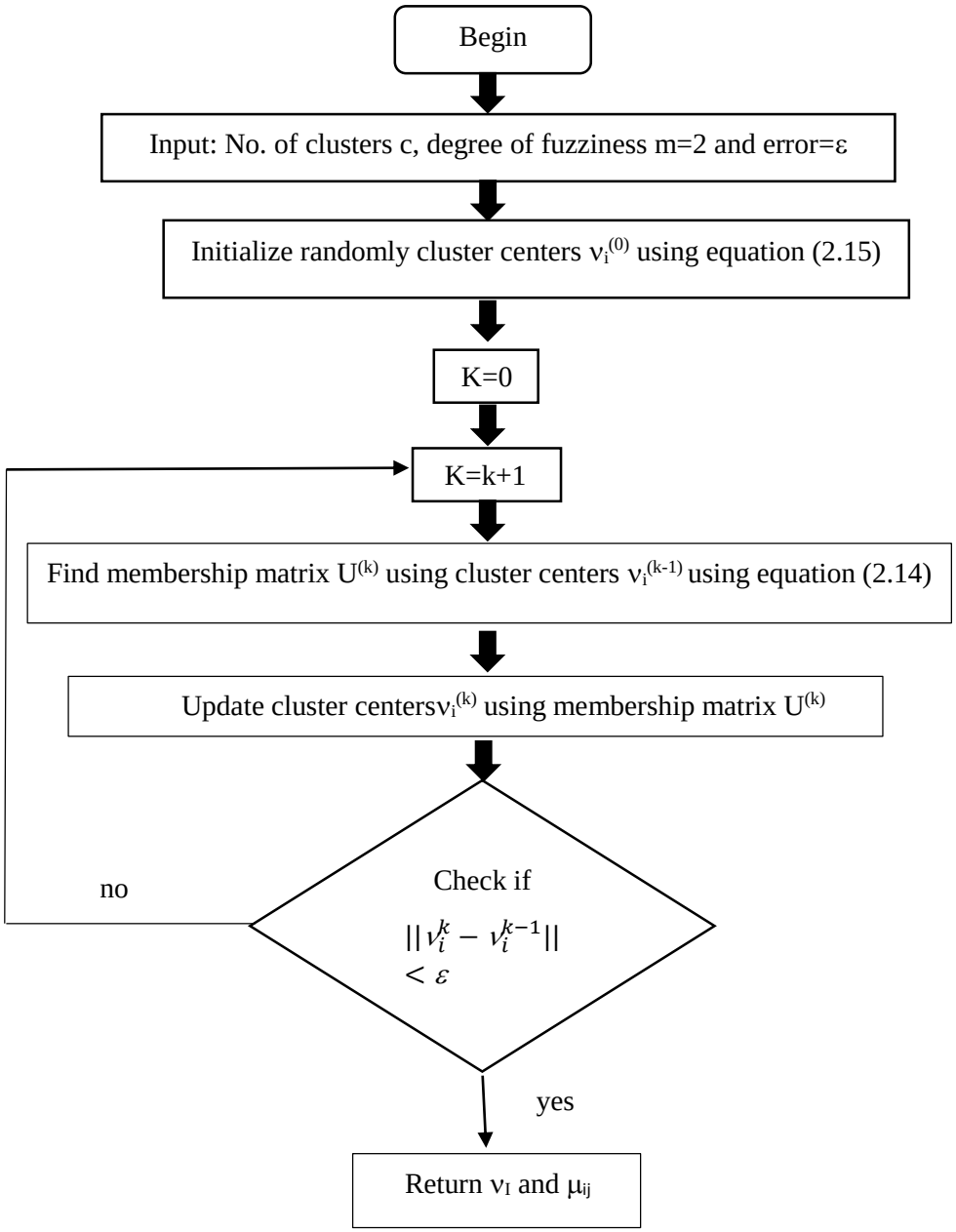

Fig 2.14 Flowchart of FCM algorithm

2.4 Results and Discussions

The performance of the proposed method is evaluated on real-patient brain MRI both qualitatively and quantitatively. The segmentation results of our proposed method have been compared with those of the standard FCM algorithm.

The proposed work has been implemented by the language of Matlab® 2015a on a personal computer with a 3.8 Ghz CPU, 4.00GB RAM under 32-bit Windows 7 operating system.

2.4.1 Dataset Description and parameter setting:

The database constitutes real-patient MRI Multiple sclerosis database (MRI MS DB) obtained from Institute of Neurology and Genetics, Nicosia, Cyprus. The transverse T2-weighted MR images were obtained using a 1.5T whole body Philips ACS NT MR imager [37-40]. 11 MRI slices from 4 patients have been used for the proposed work making a total of 44 MR images. Each image has 8-bit representation and is of size 512x512.

In the morphological pre-processing and image enhancement part, length of the linear structuring elements as well as the radius of the circular structuring element, each has been chosen to be equal to 3 units, as such a choice has been found to yield the best overall results in this study. For the FCM algorithm, the following considerations are made: degree of fuzziness m=2, maximum number of iterations=100, and minimum amount of improvement=10^{-5}. Iteration stops if maximum number of iterations is exceeded or the improvement between two consecutive iterations is equal to or less than 10^{-5}.

2.4.2 Qualitative Evaluation:

The qualitative evaluation deals with visually comparing the segmented tissue regions- white matter (WM), gray matter (GM) and cerebro-spinal fluid (CSF) based on standard FCM clustering and our proposed morphological pre-processing based FCM clustering. The images of Fig 2.15 present a visual comparison between the brain MRI segmentation results obtained using FCM only and our proposed method i.e., using a mathematical morphology based pre-processing along with FCM clustering algorithm. The images clearly show that the proposed method segments the

intricate ‘bright’ structural details of the brain like the CSF filled grooves and ventricles better than the conventional FCM clustering method directly applied on raw images. Moreover, Fig 2.16 shows a qualitative view of the segmented CSF structures of various MRI slices from a number of patients selected from the available database, by both the conventional and proposed methods and an improvement in the segmentation result is observed.

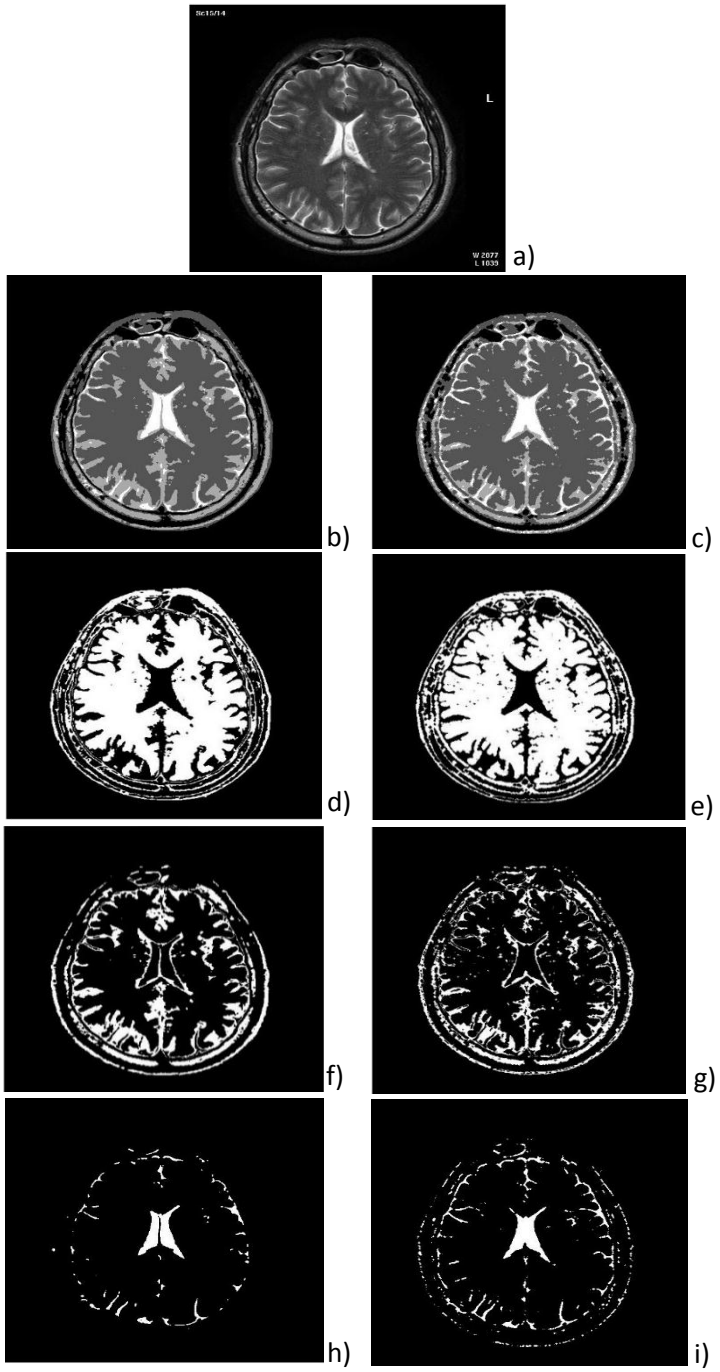

Fig 2.15 (a) original MR image, slice #14

(b),(d),(f),(h): Clustered image, WM, GM and CSF respectively using conventional FCM

(c),(e),(g),(i): Clustered image, WM, GM and CSF respectively using proposed method

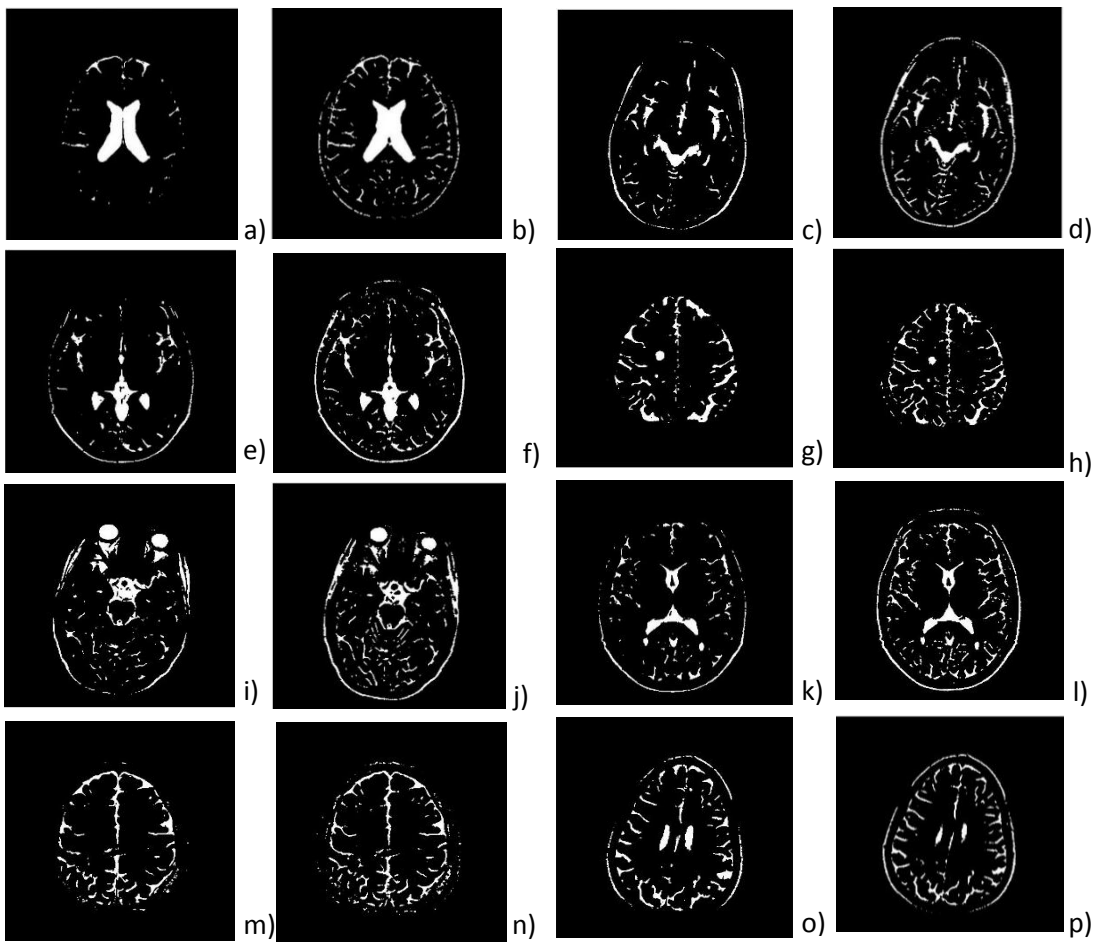

Fig 2.16 1st and 3rd column: CSF segments obtained using conventional FCM

2nd and 4th column: CSF segments obtained using proposed method.

2.4.3 Quantitative Evaluation:

As the *'ground truth'* of segmentation for real patient MRI is not readily available, quantitative analysis based on cluster validity functions have been considered only.

2.4.3.1 Cluster validity functions:

(a) *Partition coefficient (V_{pc})*: V_{pc} [34,39,34(31),34(32)]is an important indicator of fuzzy partition and provides best performance with less fuzziness. It is defined as follows:

$$V_{pc} = \frac{1}{n}\sum_{i=1}^{c}\sum_{j=1}^{n}\mu_{ij}^{2} \qquad (2.16)$$

As V_{pc} ($0 \leq V_{pc} \leq 1$) increases, the clustering becomes 'better' i.e., more optimal.

(b) *Partition Entropy (V_{pe})*: V_{pe} [38,39,34(32)] is defined as follows:

$$V_{pe} = -\frac{1}{n}\sum_{i=1}^{c}\sum_{j=1}^{n}[\mu_{ij} log \mu_{ij}] \qquad (2.17)$$

As V_{pe} ($0 \leq V_{pe} \leq 1$) decreases, the clustering becomes 'better' i.e., more optimal.

V_{pc} and V_{pe} are calculated for each image in both the cases of our proposed method and conventional FCM clustering method. The quantitative results are shown for 4 different patients in Fig 2.17 and Fig 2.18. Fig 2.19 shows the comparison of the average V_{pc} and V_{pe} values for each of the 4 patients.

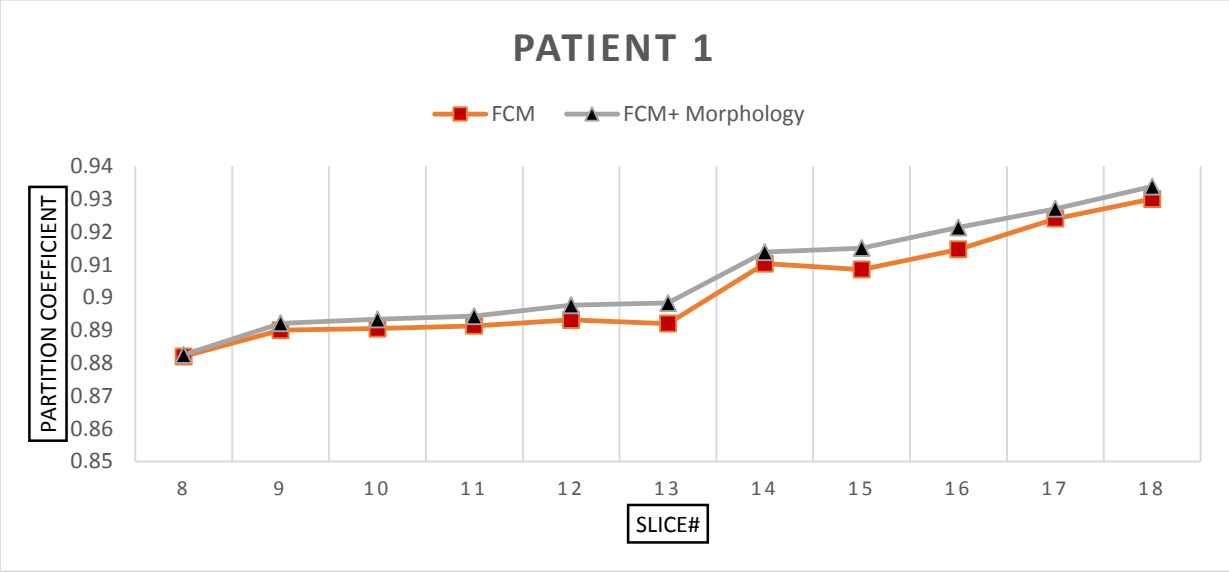

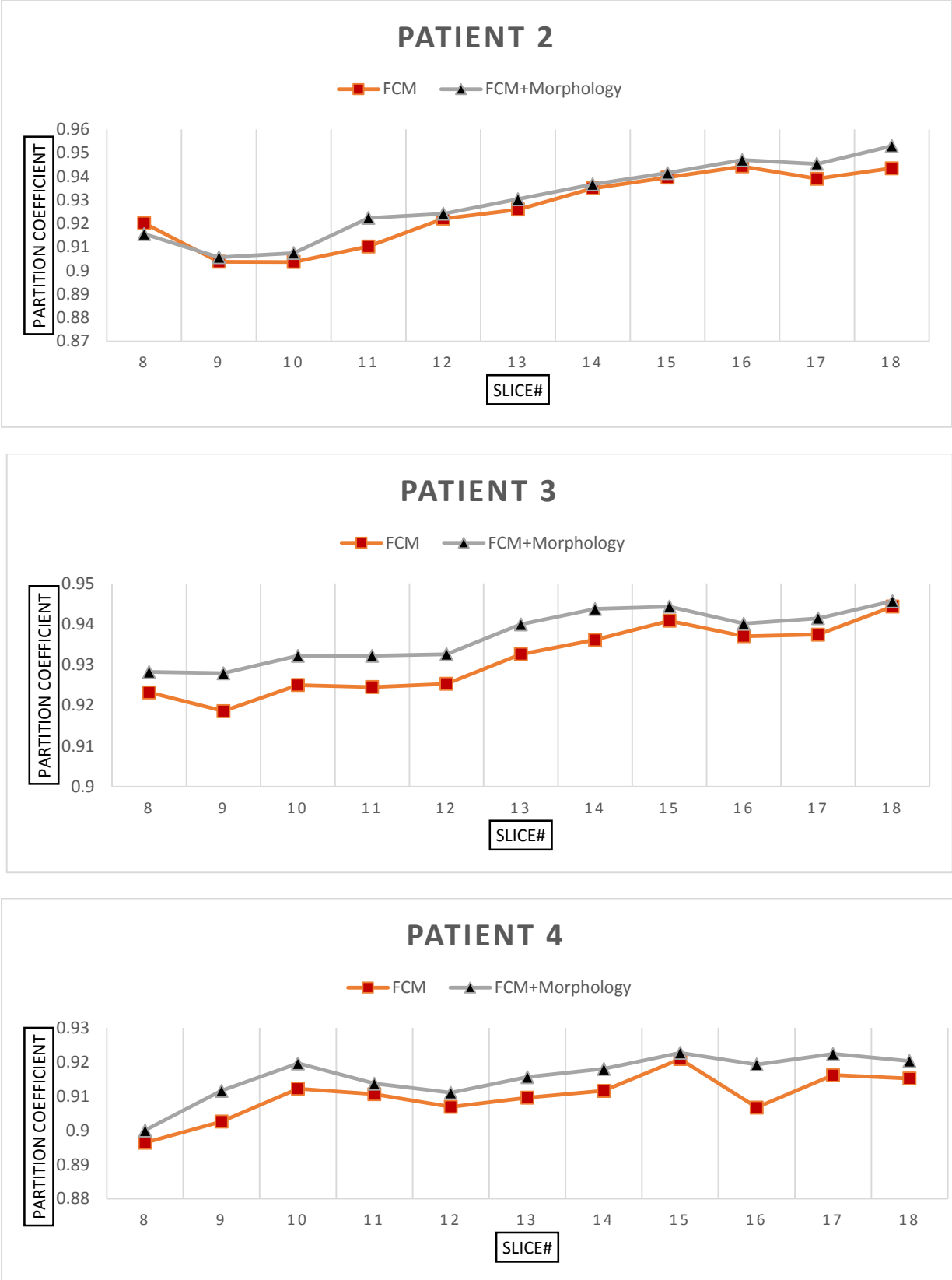

Fig 2.17 Partition coefficient values for the proposed method and conventional FCM

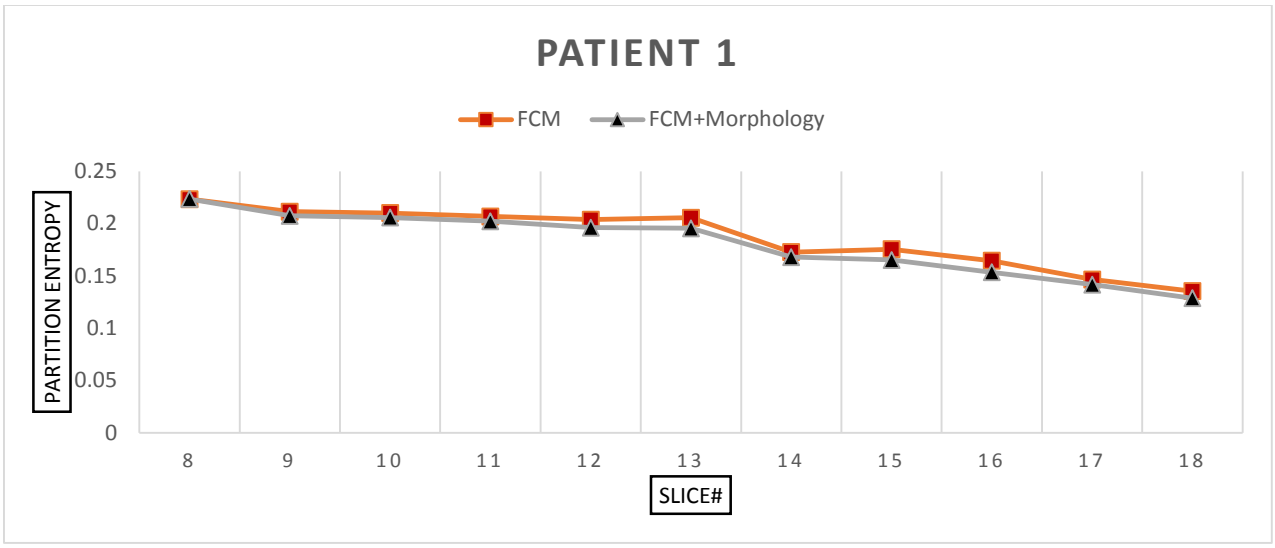
PATIENT 1
FCM
FCM+Morphology
PARTITION ENTROPY
0.25
0.2
0.15
0.1
0.05
0
8
9
10
11
12
13
14
15
16
17
18
SLICE#

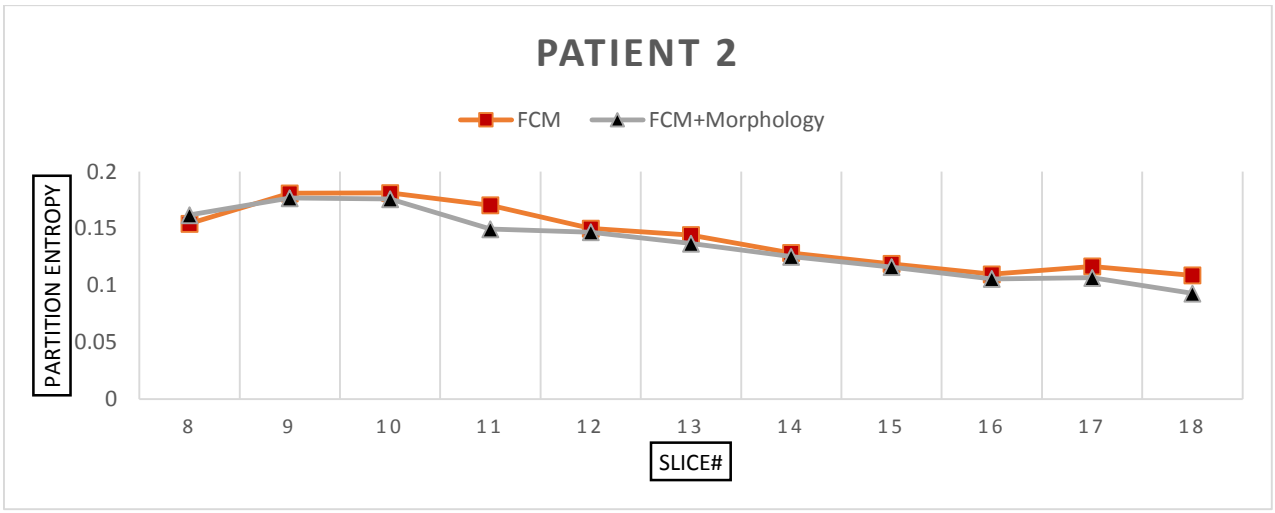
PATIENT 2
FCM
FCM+Morphology
PARTITION ENTROPY
0.2
0.15
0.1
0.05
0
8
9
10
11
12
13
14
15
16
17
18
SLICE#

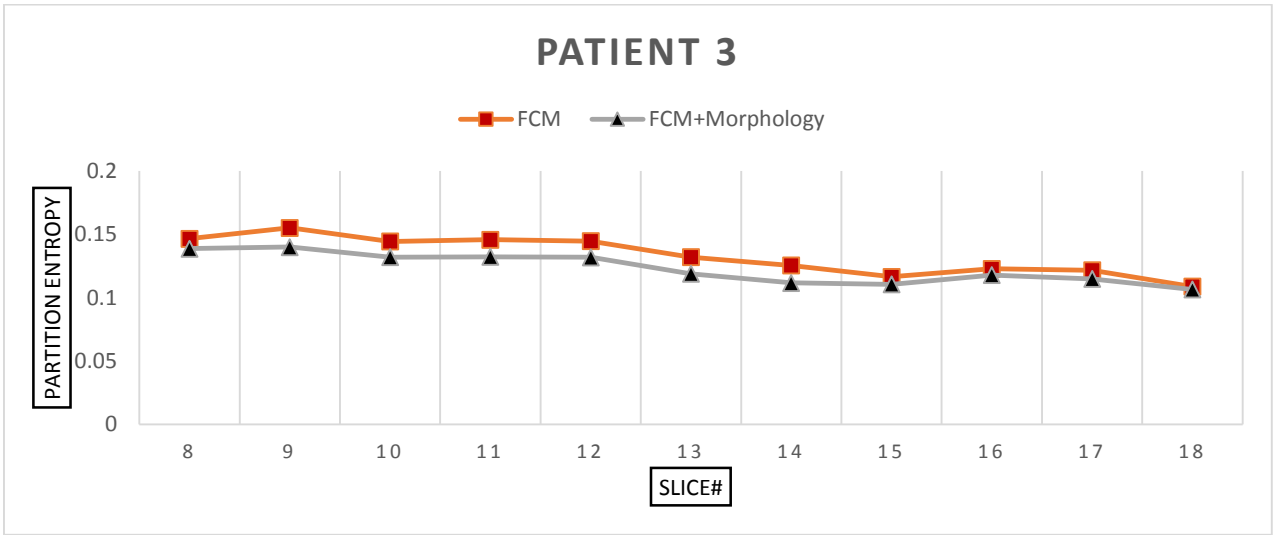
PATIENT 3
FCM
FCM+Morphology
PARTITION ENTROPY
0.2
0.15
0.1
0.05
0
8
9
10
11
12
13
14
15
16
17
18
SLICE#

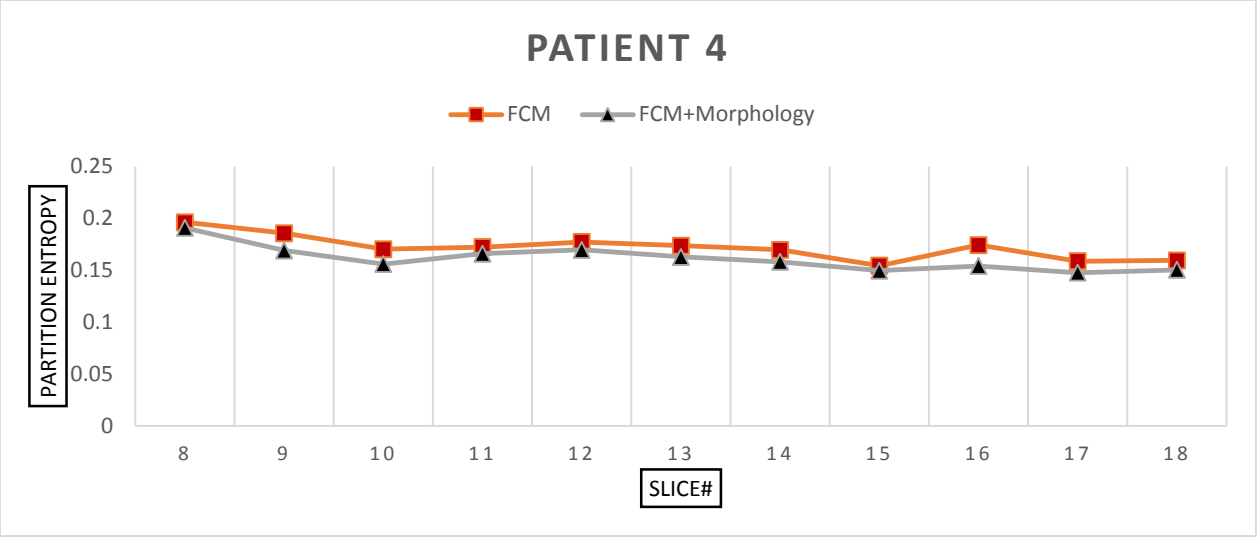

Fig 2.18 Partition entropy values for the proposed method and conventional FCM

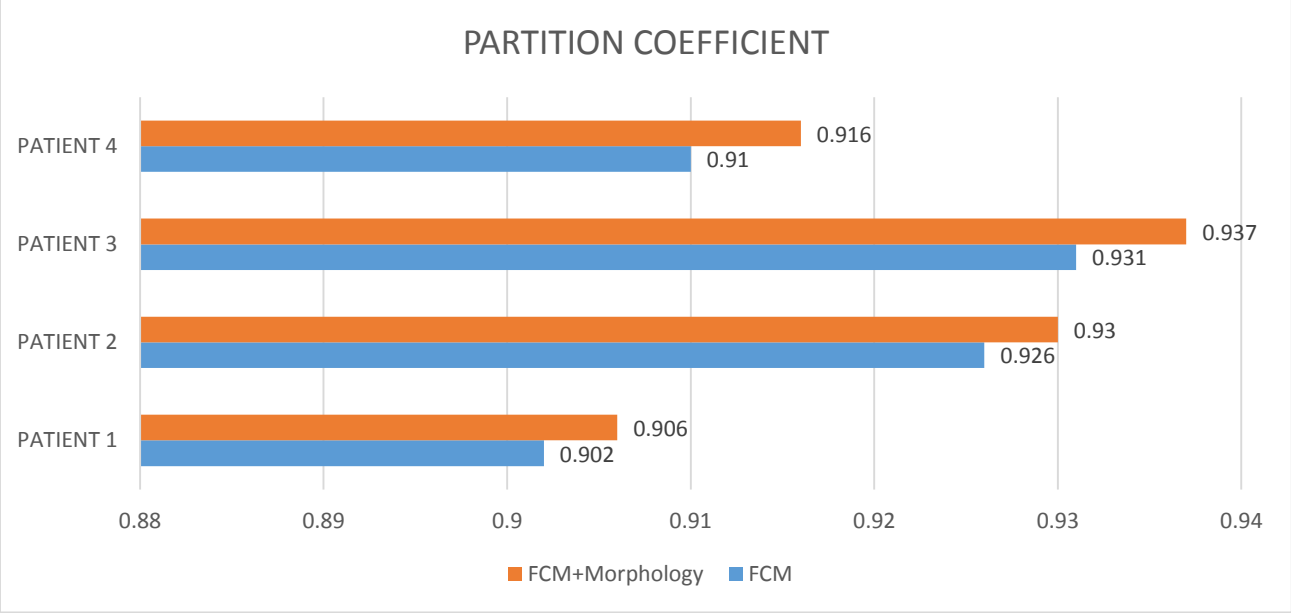

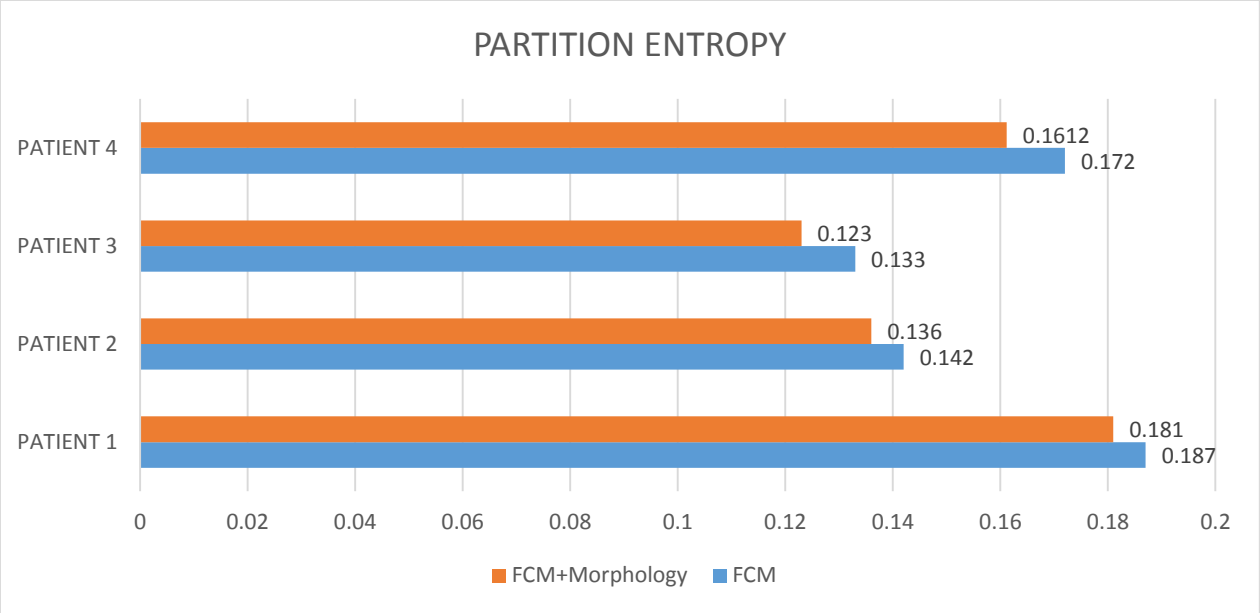

Fig 2.19 Comparison of average Partition Coefficient (V_{pc}) and average Partition Entropy (V_{pe}) values for the proposed method and conventional FCM

As shown in Fig 2.17, the V_{pc} values as produced by the proposed method, is higher for each MRI slice, for each patient. From Fig 2.18, it can also be seen that the proposed method has yielded lower V_{pe} values for each MRI slice, for each patient. The only exception is slice no. 8 of patient no. 2 where the proposed method has produced a slightly worse value for both V_{pc} and V_{pe}. Hence, it can be said that for both V_{pc} and V_{pe} our proposed method comprising of morphological pre-processing, has resulted in better clustering results in comparison to the case where clustering has been done solely with the help of conventional FCM without applying image enhancement. Moreover, from Fig 2.19 it can also be seen that for each patient, the average V_{pc} and V_{pe} values, taken over the 11 MRI slices, are better in comparison to the conventional FCM method applied on raw images.

2.5 Conclusions

In this chapter, a novel and simple mathematical morphology based method has been studied for the purpose of real-patient brain MR image enhancement. The technique comprises of the

application of morphological operators like *opening*, *closing* and *tophat* filtration to the brain MRI slices of real patients for the purpose of noise removal and contrast enhancement. Conventional Fuzzy C-means (FCM) clustering method has then been applied to the enhanced brain MRI slices to segment the image into three segments i.e., white matter (WM), gray matter (GM) and cerebrospinal fluid (CSF). Qualitative analysis has shown that the proposed method does a better job in extracting the intricate and 'bright' CSF structures than the conventional FCM clustering method on raw MR images. Moreover, in absence of the availability of MRI segmentation '*ground truth*', cluster validity functions like partition coefficient (V_{pc}) and partition entropy (V_{pe}) have been employed to check the performance of the proposed method over conventional FCM clustering. It has been observed that the proposed method also yields better clustering results in comparison to the conventional FCM clustering on raw MR images.

References

[1] Pierre Soille. “Morphological Image Analysis Principles and Applications”. Springer- Verlag Berlin Heidelberg Publications, New York, 2004.

[2] Robert M. Haralick, Stanley R. Sternberg and Xinhua Zhuang. “Image Analysis using Mathematical Morphology”. IEEE Trans. on Pattern Analysis and Machine Intelligence, Vol. PAMI-4, no. 4, July, 1987, pp.532-550.

[3] Luc Vincent. “Morphological Grayscale Reconstruction in Image Analysis: Applications and Efficient Algorithms”. IEEE Trans. on Image Processing, Vol. 2, no. 2, April, 1993, pp.176-201.

[4] Martino Pesaresi and Jon Atli Benediktsson. “A New Approach for the Morphological Segmentation of High-Resolution Satellite Imagery”. IEEE Trans. on Geoscience and Remote Sensing, Vol. 39, no. 2, February, 2001, pp.309-320.

[5] Miguel A. Luengo-Oroz, Emmanuel Faure and Jesús Angulo. “Robust Iris Segmentation on Uncalibrated Noisy Images using Mathematical Morphology”. Image and Vision Computing 28 (2009), 278-284.

[6] Shen Pan and Mineichi Kudo. “Segmentation of Pores in Wood Microscopic Images based on Mathematical Morphology with a Variable Structuring Element”. Computers and Electronics in Agriculture 75 (2011), 250-260.

[7] Anders Landström and Matthew J. Thurley. “Morphology-Based Crack Detention for Steel Slabs”. IEEE Journal of Selected Topics in Image Processing, Vol. 6, no. 7, November, 2012, pp.866-875.

[8] Laura Gui, Radoslaw Lisowski, Tamara Faundez, Petra S. Hüppi, François Lazeyras and Michel Kocher. “Morphology-driven Automatic Segmentation of MR Images of the Neonatal Brain”. Medical Image Analysis 16 (2012), 1565-1579.

[9] Sandra Morales, Valery Naranjo, Jesús Angulo and Mariano Alcañiz. “Automatic Detection of Optic Disc Based on PCA and Mathematical Morphology”. IEEE Trans. on Medical Imaging, Vol. 32, no. 4, April, 2013, pp.786-796.

[10] Andrés Serna and Beatriz Marcotegui. “Detection, Segmentation and Classification of 3D Urban Objects using Mathematical Morphology and Supervised Learning”. ISPRS Journal of Photogrammetry and Remote Sensing 93 (2014), 243-255.

[11] Isabelle Bloch and Henri Maître. “Fuzzy Mathematical Morphologies: A Comparative Study”. Pattern Recognition, Vol. 28, No. 9, pp. 1341-1387, 1995.

[12] Maofu Liu, Ya Liu, Huijun Hu and Liqiang Nie. “Genetic Algorithm and Mathematical Morphology Based Binarization Method for Strip Steel Defect Image with Non-Uniform Illumination”. J. Vis. Commun. Image R. 37 (2016), 70–77.

[13] Rik Stokking, Koen L. Vincken, and Max A. Viergever. “Automatic Morphology-Based Brain Segmentation (MBRASE) from MRI-T1 Data”. NeuroImage 12, 726–738 (2000).

[14] Mike Nachtegael and Etienne E. Kerre. “Connections between Binary, Gray-Scale and Fuzzy Mathematical Morphologies”. Fuzzy Sets and Systems 124 (2001), 73–85.

[15] Eduardo Blotta, Agustina Bouchet, Marcel Brun and Virginia Ballarin. “Characterization of Bio-Dynamic Speckles through Classical and Fuzzy Mathematical Morphology Tools”. Signal Processing 93 (2013), 1864–1870.

[16] S. Valero, J. Chanussot , J.A. Benediktsson, H. Talbot and B. Waske. “Advanced Directional Mathematical Morphology for the Detection of the Road Network in Very High Resolution Remote Sensing Images”. Pattern Recognition Letters 31 (2010), 1120–1127.

[17] Vladimir Ćurić , Anders Landström, Matthew J. Thurley and Cris L. Luengo Hendriks. “Adaptive Mathematical Morphology – A Survey of the Field”. Pattern Recognition Letters 47 (2014), 18–28.

[18] Eysteinn Már Sigurðsson, Einar Stefánsson, Silvia Valero, Jón Atli Benediktsson, Jocelyn Chanussot and Hugues Talbot. “Automatic Retinal Vessel Extraction Based on Directional Mathematical Morphology and Fuzzy Classification”. Pattern Recognition Letters 47 (2014), 164–171.

[19] B. Bouraoui, C. Ronsea, J. Baruthio, N. Passat and P. Germain. “3D Segmentation of Coronary Arteries Based on Advanced Mathematical Morphology Techniques”. Computerized Medical Imaging and Graphics 34 (2010), 377–387.

[20] Gehad Hassana, Nashwa El-Bendary, , Aboul Ella Hassanien, Ali Fahmy, Abullah M.Shoeb and Vaclav Snasel. “Retinal Blood Vessel Segmentation Approach Based on Mathematical Morphology”. Procedia Computer Science 65 (2015), 612-622. International Conference on Communication, Management and Information Technology (ICCMIT 2015).

[21] Eyad Haj Said, Diaa Eldin M. Nassar and Gamal Fahmy. “Teeth Segmentation in Digitized Dental X-Ray Films using Mathematical Morphology”. IEEE Trans. on Information Forensics and Security, Vol. 1, no. 2, June, 2006, pp.178-189.

[22] Ben-Shung Chow. “Mathematical Morphology for Applications to Sensor Networks”. IEEE Sensors Journal, Vol. 12, no. 12, December, 2012, pp.3473-3479.

[23] J. Pastore, A. Bouchet, E. Moler and V. Ballarin. “Segmentation of Bone Marrow Biopsies by Mathematical Morphology in Color Spaces”. IEEE Latin America Trans., Vol. 11, no. 1, February, 2013, pp.329-333.

[24] Li Yu and Runsheng Wang. “Shape Representation Based on Mathematical Morphology”. Pattern Recognition Letters 26 (2005), 1354–1362.

[25] Benoît Naegel. “Using Mathematical Morphology for the Anatomical Labeling of Vertebrae from 3D CT-Scan Images”. Computerized Medical Imaging and Graphics 31 (2007), 141–156.

[26] Stelios Halkiotis, Taxiarchis Botsis and Maria Rangoussi. “Automatic Detection of Clustered Microcalcifications in Digital Mammograms using Mathematical Morphology and Neural Networks”. Signal Processing 87 (2007), 1559–1568.

[27] Editorial. “Special Issue on Advances in Mathematical Morphology”. Pattern Recognition Letters 47 (2014), 1–2.

[28] Antonio Jimeno-Morenilla, Rafael Molina-Carmona and Jose-Luis Sanchez-Romeroa. “Mathematical Morphology for Design and Manufacturing”. Mathematical and Computer Modelling 54 (2011), 1753–1759.

[29] Daniel Welfer, Jacob Scharcanski and Diane Ruschel Marinho. “Fovea Center Detection Based on the Retina Anatomy and Mathematical Morphology”. Computer Methods and Programs in Biomedicine 104 (2011), 397–409.

[30] A. Dufour, O. Tankyevych, B. Naegel, H. Talbot, C. Ronse, J. Baruthio, P. Dokládal and N. Passat. “Filtering and Segmentation of 3D Angiographic Data: Advances Based on Mathematical Morphology”. Medical Image Analysis 17 (2013), 147–164.

[31] S. Ramathilagam, R. Pandiyarajan, A. Sathya, R. Devi and S. R. Kannan. “Modified Fuzzy C-Means Algorithm for Segmentation of T1-T2-Weighted Brain MRI”. Journal of Computational and Applied Mathematics 235 (2011), 1758-1586.

[32] Karan Sikka, Nitesh Sinha, Pankaj K. Singh and Amit K. Mishra. "A Fully Automated Algorithm under Modified FCM Framework for Improved Brain MR Image Segmentation". Magnetic Resonance Imaging 27 (2009), 994-1004.

[33] Jianzhong Wang, Jun Kong, Yinghua Lu, Miao Qi and Baoxue Zhang. "A Modified FCM Algorithm for MRI Brain Image Segmentation using Both Local and Non-Local Spatial Constraints". Computerized Medical Imaging and Graphics 32 (2008), 685–698.

[34] Sudip Kumar Adhikari, Jamuna Kanta Sing, Dipak Kumar Basu and Mita Nasipuri. "Conditional Spatial Fuzzy C-Means Clustering Algorithm for Segmentation of MRI Images". Applied Soft Computing 34 (2015), 758–769.

[35] Hanuman Verma, R.K. Agrawal and Aditi Sharan. "An Improved Intuitionistic Fuzzy C-Means Clustering Algorithm Incorporating Local Information for Brain Image Segmentation". Applied Soft Computing J. (2015), 1-15.

[36] Cunyong Qiu, Jian Xiao, Long Yu, Lu Han and Muhammad Naveed Iqbal. "A Modified Interval Type-2 Fuzzy C-Means Algorithm with Application in MR Image Segmentation". Pattern Recognition Letters 34 (2013), 1329-1338.

[37] C.P. Loizou, S. Petroudi, I. Seimenis, M. Pantziaris and C.S. Pattichis. "Quantitative Texture Analysis of Brain White Matter Lesions Derived from T2-Weighted MR Images in MS Patients with Clinically Isolated Syndrome". Journal of Neuroradiology (2014), 1-16.

[38] C.P. Loizou, V. Murray, M.S. Pattichis, I. Seimenis, M. Pantziaris, C.S. Pattichis, "Multi- scale amplitude modulation-frequency modulation (AM-FM) texture analysis of multiple sclerosis in brain MRI images," IEEE Trans. Inform. Tech. Biomed., vol. 15, no. 1, pp. 119-129, 2011.

[39] C.P. Loizou, E.C. Kyriacou, I. Seimenis, M. Pantziaris, S. Petroudi, M. Karaolis, C.S. Pattichis, "Brain white matter lesion classification in multiple sclerosis subjects for the prognosis of future disability," Intelligent Decision Technologies Journal (IDT), vol. 7, pp. 3-10, 2013.

[40] C.P. Loizou, M. Pantziaris, C.S. Pattichis, I. Seimenis, "Brain MRI Image normalization in texture analysis of multiple sclerosis", J. Biomed. Graph. & Comput., vol. 3, no.1, pp. 20-34, 2013.

[41] Zhimin Wang, Qing Song b, Yeng Chai Soh and Kang Sim. "An Adaptive Spatial Information-Theoretic Fuzzy Clustering Algorithm for Image Segmentation". Computer Vision and Image Understanding 117 (2013), 1412-1420.

[42] R. C. Gonzalez and R. E. Woods, "Digital Image Processing", Pearson Education, 2008.

[43] Maintz, J.B.A, Digital and Medical Image Processing, Lecture Notes, Utrecht University.

CHAPTER 3

MULTILEVEL OPTIMAL THRESHOLDING OF BRAIN MRI USING MODIFIED HYBRIDIZED BAT ALGORITHM

3.1 Introduction

Metaheuristic algorithms are genuinely creative in exploring paths to a solution and are becoming extremely popular, robust and powerful methods for solving many tough optimization problems. The vast majority of such algorithms have been inspired or derived from the behavior of biological systems and/or physical systems, such as simulated annealing (SA), particle swarm optimization (PSO), differential evolution (DE), genetic algorithm (GA), harmony search (HS), artificial bee colony algorithm (ABC), firefly algorithm (FA), cuckoo search algorithm (CS) etc. Algorithms such as GA, PSO, DE are very useful but they are not fully capable in dealing with multimodal optimization problems [14]. The attraction behavior, light intensity coding and distance dependence based FA [19] provides a surprising capability to deal with non-linear, multimodal optimization problems efficiently [14]. The CS algorithm based on the brooding behavior of some cuckoo species has very good convergence behavior [14].

The Bat Algorithm (BA) is a comparatively recent and very promising metaheuristic algorithm proposed by X.S Yang in 2010 [1]. It is based on the echolocation behavior of microbats and has found a wide application in various types of optimization problems in recent times. The properties of bat algorithm that gives it an edge over other recent metaheuristic algorithms are: frequency tuning, automatic zooming and parameter control [1,14]. Huang et al. [32] used BA for solving large scale optimization problems. Khan et al. [33] proposed a fuzzy clustering algorithm based on BA for ergonomic screening of office workplaces. Horng et al. [34] used a chaotic levy flight based BA for parameter estimation in nonlinear dynamic biological systems. Zhang et al. [35] developed an image matching technique using BA with mutation. Bing Meng et al. [7] proposed a novel bat algorithm with habitat selection and Doppler Effect to solve optimization problems. Karri et al. [8] utilized BA for image compression. Gao et al. [10] proposed a novel visual tracking method using BA. Adarsh et al. [11] used chaotic BA for economic load dispatch. Coelho et al.

[12] proposed an enhanced BA approach for reducing electrical power consumption of air conditioning systems. Osaba et al. [9] used an improved version of discrete BA for symmetric and asymmetric travelling salesman problem.

Multilevel image thresholding is a very important image processing technique that is used to subdivide an image into disjoint sets of pixels sharing similar properties such as intensity, color or texture on the basis of optimally selected thresholds. The various different methods for calculating optimum image thresholds include maximizing gray level variance [36], entropy [37], similarity [38] and measure of fuzziness [39]. Among all these, the entropy of the image histogram is the most popular optimization method. Over the last decade there has been a remarkable achievement in multilevel image thresholding using fuzzy entropy based objective functions [21-27].

Bat algorithm has been utilized in a few recent works for multilevel image thresholding. Alihodzic et al. [5] proposed an improved bat algorithm based on Kapur's entropy and Otsu's criterion for image thresholding. Ye et al. [6] used a fuzzy entropy based bat algorithm for optimal thresholding of conventional benchmark images. In both the works, the authors have compared the results obtained from bat algorithm with the results of other metaheuristic nature-inspired algorithms like PSO, DE, CS, FA, GA, ABC, ACO and concluded that the bat algorithm based methods produced overall better results. But the bat algorithm suffers from a drawback that at times it tends to get trapped into local optima and this becomes a great problem when a large number of thresholds are to be dealt with. In the present chapter an attempt has been made to overcome this drawback by proposing a modified hybridized bat algorithm for multilevel thresholding of brain MR images and the fuzzy entropy of the image histogram has been used as the objective function. Finally, a comparison has been made between the segmentation results obtained from the basic version of the bat algorithm with the hybridized method.

The rest of the chapter is organized as follows. In section 3.2 the entropy based image thresholding method is discussed. Section 3.3 deals with the basic bat algorithm adapted for multilevel image thresholding. In section 3.4 the proposed hybridized bat algorithm is discussed in details. The detailed results and discussions are portrayed in section 3.5. Finally, the chapter is concluded in section 3.6.

3.2 Entropy based Multilevel Image Thresholding

3.2.1 Overview:

Multilevel image thresholding is the process where an image is segmented into *n*+1 distinct regions using n distinct image intensity values called thresholds. Let us consider a gray scale image I as a set of pixels A, multilevel thresholding can be defined as dividing the set A into *n*+1 disjoint subsets (A_0, A_1, …., A_n) by some numbers which are nothing but gray intensity values (t_0, t_1, …., t_{n-1}) such that [5]

$$A_0 = \{(x,y): 0 \le f(x,y) < t_0\},$$

$$A_1 = \{(x,y): t_0 \le f(x,y) < t_1\},$$

$$A_2 = \{(x,y): t_1 \le f(x,y) < t_2\}, \quad (3.1)$$

.

.

.

$$A_n = \{(x,y): t_{n-1} \le f(x,y) \le L-1\},$$

where (x, y) is a pixel defined by coordinates x and y in the Cartesian coordinate system, f(x, y) represents the gray value corresponding to pixel (x, y). For an 8-bit digital image $L = 2^8$, thus f(x) takes values in the range [0, 255]. The aim of any multilevel thresholding problem is to calculate the optimal threshold values (t_0, $t_1 \ldots t_{n-1}$). Thus,

$$\forall \text{ i, j} \qquad A_i \cap A_j = \emptyset \quad \text{and} \qquad \bigcup_{i=0}^{n} A_i = I \quad (3.2)$$

In information theory, entropy measures the amount of uncertainty of an unknown or random quantity. The entropy-based thresholding methods are derived from maximization of Shannon's entropy. Entropic thresholding " considers the image foreground and background as two different signal sources, so that when the sum of the two class entropies reaches its maximum, the image is said to be optimally thresholded " [28]. The different variations of the entropic thresholding methods are Pun entropy [40, 41], Kapur entropy [29], Yen entropy [42], Johannasen entropy [43], Sahoo entropy [44], Mello entropy [45], Silva entropy [46], Kullback cross-entropy [47], Li cross-entropy [48], Attas cross-entropy [49], Osaimi cross-entropy [50], Saeed cross-entropy [51], Brink cross-entropy [52], Pal cross-entropy [53], Ajlan cross-entropy [54], Shanbag fuzzy-entropy [55], Cheng fuzzy-entropy [25], Zhao fuzzy-entropy [25], Tao fuzzy-entropy [22]. Out of all these

entropic methods, Kapur entropy and Tao fuzzy-entropy have found the most prominence in finding optimal thresholds for multilevel image thresholding.

Image processing has to deal with many ambiguous situations and the fuzzy set theory is a useful mathematical tool for handling such ambiguity or uncertainty. For this reason, the fuzzy entropy based method has found an edge over other methods and there have been numerous applications of fuzzy entropies in image segmentation.

3.2.2 Fuzzy entropy based multilevel image thresholding:

A fuzzy entropy is a function on fuzzy sets that becomes smaller when the sharpness of its argument fuzzy set is improved [22]. The concept of entropy in the theory of fuzzy sets was first introduced by Luca and Termini in 1972. Afterwards it has been successfully implemented to solve numerous image thresholding problems. Zhao et al.,2001 established the relation between probability partition (PP) and entropy based fuzzy c-partition (FP) in image thresholding. Tao et al., 2003 [22] first designed a three-level thresholding method based on this concept of fuzzy entropy for image segmentation.

Let D={(x,y):x=0,1,…,*M*-1;y=0,1,…,*N*-1} and G={0,1,…,*L*-1}, where *M*,*N* and *L* are three positive integers standing for width (in pixels), height (in pixels) and maximum gray level intensity of the image. Hence,

I(x,y)∈G $\forall$ (x,y)∈D where $0 \leq I(x,y) \leq L-1$ is the gray level value of the image at the pixel (x,y).

So the image can be mapped in a way I: D→G.

$$D_k = \{(x,y): I(x,y) = k, (x,y) \in D, k = 0,1,2, \dots, L-1\} \quad (3.3)$$

Let the histogram of the given image be H = {h_0, h_1, …., h_{L-1}} where h_k represents the number of pixels having gray level intensity equal to k. The normalized value h_{nk} is given as:

$$h_{nk} = \frac{h_k}{M*N} \qquad k=0, 1, 2\ldots., L-1 \quad (3.4)$$

$$0 \leq h_{nk} \leq 1, \qquad \text{and} \qquad \sum_{k=0}^{L-1} h_{nk} = 1 \quad (3.5)$$

If p_k is the probability of occurrence of the gray level k in the image, then $p_k = h_{nk}$.

Our objective is to classify domain D of the gray level image of interest into three classes E_d, E_m and E_b. E_d consists of 'dark' pixels i.e pixels of 'low' gray level intensity, E_m consists of 'medium' intensity value pixels and E_b consists of 'bright' pixels i.e pixels of 'high' gray level intensity. $\Pi_3 = \{E_d, E_m, E_b\}$ [24] is an unknown probabilistic partition of D whose probability distribution is given by

$$p_d = PE_d) \text{ , } p_m = P(E_m), \; p_b = P(E_b). \tag{3.6}$$

A fuzzy set is an extension of a crisp set. In a fuzzy set an element may partially belong to a set. Let A be a fuzzy set, where $A \subset X$ is defined as $A=\{(x,\mu_A(x))|x \in X\}$, where $0 \leq \mu_A(x) \leq 1$ is called the membership function which defines to what extent x belongs to A.

Three functions- the $Z(k,a_1,b_1,c_1)$-function, $U(k,a_1,b_1,c_1,a_2,b_2,c_2)$ and $S(k,a_2,b_2,c_2)$-function (Fig. 3.1) are used to approximate the memberships of μ_d, μ_m and μ_b of our image with $2^8=256$ gray levels. The two thresholds T_1 and T_2 for three-level image thresholding depend on the values of these six parameters, namely, a_1, b_1, c_1, a_2, b_2, c_2 [22]. Hence, the objective is to find these six parameters such that the required optimum thresholds T_1 and T_2 are obtained. The following conditions must be satisfied:

$$0 \leq a_1 \leq b_1 \leq c_1 \leq a_2 \leq b_2 \leq c_2 \leq 255.$$

For each k=0, 1, 2, …., 255; let

$$\begin{aligned} D_{kd} &= \{(x,y): I(x,y) \leq T_1, (x,y) \in D_k\} \\ D_{km} &= \{(x,y): T_1 < I(x,y) \leq T_2, (x,y) \in D_k\} \\ D_{kb} &= \{(x,y): I(x,y) > T_2, (x,y) \in D_k\} \end{aligned} \tag{3.7}$$

Then,

$$\begin{aligned} P_{kd} &= P(D_{kd}) = p_k * p_{d|k} \\ P_{km} &= P(D_{km}) = p_k * p_{m|k} \\ P_{kb} &= P(D_{kb}) = p_k * p_{b|k} \end{aligned} \tag{3.8}$$

where, $p_{d|k}$, $p_{m|k}$ and $p_{d|k}$ are the conditional probability that a pixel belongs to fuzzy sets 'dark', 'medium' and 'bright' respectively provided it has a gray level intensity equal to *k*, subject to a constraint $p_{d|k} + p_{m|k} + p_{d|k} = 1$ (k=0, 1, 2, …, 255). '*' denotes scalar multiplication.

$$P_d = P(E_d) = \sum_{k=0}^{255} P(D_{kd})$$

$$= \sum_{k=0}^{255} P(D_k) * P(E_d|D_k) = \sum_{k=0}^{255} p_k * p_{d|k}$$

$$P_m = P(E_m) = \sum_{k=0}^{255} P(D_{km})$$

$$= \sum_{k=0}^{255} P(D_k) * P(E_m|D_k) = \sum_{k=0}^{255} p_k * p_{m|k} \quad (3.9)$$

$$P_b = P(E_b) = \sum_{k=0}^{255} P(D_{kb})$$

$$= \sum_{k=0}^{255} P(D_k) * P(E_b|D_k) = \sum_{k=0}^{255} p_k * p_{b|k}$$

It is considered that the conditional probabilities are same as the membership values of a pixel with intensity k to belong to the fuzzy sets 'dark', 'medium' and 'gray'. Thus $p_{d|k}$, $p_{m|k}$, $p_{d|k}$ are same as μ_d, μ_m and μ_b respectively. So, it can be concluded:

$$p_d = \sum_{k=0}^{255} p_k * \mu_d(k)$$

$$p_m = \sum_{k=0}^{255} p_k * \mu_m(k) \quad (3.10)$$

$$p_b = \sum_{k=0}^{255} p_k * \mu_b(k)$$

As shown in Fig.3.1, the Z(k,a_1,b_1,c_1)-function, U($k,a_1,b_1,c_1,a_2,b_2,c_2$)-function and S($k,a_2,b_2,c_2$)-function act as the membership function $\mu_d(k)$, $\mu_m(k)$ and $\mu_b(k)$ respectively. They are given as follows:

$$\mu_d(k) = \begin{cases} 1 & k \le a_1 \\ 1 - \frac{(k-a_1)^2}{(c_1-a_1)*(b_1-a_1)} & a_1 < k \le b_1 \\ \frac{(k-c_1)^2}{(c_1-a_1)*(c_1-b_1)} & b_1 < k \le c_1 \\ 0 & k > c_1 \end{cases}$$

$$\mu_m(k) = \begin{cases} 0 & k \le a_1 \\ \frac{(k-a_1)^2}{(c_1-a_1)*(b_1-a_1)} & a_1 < k \le b_1 \\ 1 - \frac{(k-c_1)^2}{(c_1-a_1)*(c_1-b_1)} & b_1 < k \le c_1 \\ 1 & c_1 < k \le a_2 \\ 1 - \frac{(k-a_2)^2}{(c_2-a_2)*(b_2-a_2)} & a_2 < k \le b_2 \\ \frac{(k-c_2)^2}{(c_2-a_2)*(c_2-b_2)} & b_2 < k \le c_2 \\ 0 & c_2 < k \end{cases} \quad (3.11)$$

$$\mu_b(k) = \begin{cases} 0 & k \le a_2 \\ \frac{(k-a_2)^2}{(c_2-a_2)*(b_2-a_2)} & a_2 < k \le b_2 \\ 1 - \frac{(k-c_2)^2}{(c_2-a_2)*(c_2-b_2)} & b_2 < k \le c_2 \\ 1 & k > c_2 \end{cases}$$

The fuzzy entropy function of each of the three classes are given as follows [22] :

$$H_d = -\sum_{k=0}^{255} \frac{p_k * \mu_d(k)}{p_d} * \ln\left(\frac{p_k * \mu_d(k)}{p_d}\right)$$

$$H_m = -\sum_{k=0}^{255} \frac{p_k * \mu_m(k)}{p_m} * \ln\left(\frac{p_k * \mu_m(k)}{p_m}\right) \quad (3.12)$$

$$H_d = -\sum_{k=0}^{255} \frac{p_k * \mu_b(k)}{p_b} * \ln\left(\frac{p_k * \mu_b(k)}{p_b}\right)$$

The total fuzzy entropy is then calculated by summing up the fuzzy entropy of each class as:

$$H(a_1, b_1, c_1, a_2, b_2, c_2) = H_d + H_m + H_b \quad (3.13)$$

The objective of this work is to find the optimal combination of these six parameters a_1, b_1, c_1, a_2, b_2 and c_2 such that $H(a_1, b_1, c_1, a_2, b_2, c_2)$ is maximum. Then the most appropriate thresholds T_1 and T_2 which segment the image into three classes can be computed as follows:

$$\mu_d(T_1) = \mu_m(T_1) = 0.5$$

$$\mu_m(T_2) = \mu_b(T_2) = 0.5 \quad (3.14)$$

Based on the formulas the solution can be given as:

$$T_1 = \begin{cases} a_1 + \sqrt{(c_1 - a_1) * (b_1 - a_1)/2} & (a_1 + c_1)/2 \le b_1 \le c_1 \\ c_1 - \sqrt{(c_1 - a_1) * (c_1 - b_1)/2} & a_1 \le b_1 \le (a_1 + c_1)/2 \end{cases}$$

$$T_2 = \begin{cases} a_2 + \sqrt{(c_2 - a_2) * (b_2 - a_2)/2} & (a_2 + c_2)/2 \le b_2 \le c_2 \\ c_2 - \sqrt{(c_2 - a_2) * (c_2 - b_2)/2} & a_2 \le b_2 \le (a_2 + c_2)/2 \end{cases} \quad (3.15)$$

It can be seen that for maximum fuzzy entropy based thresholding each threshold corresponds to 3 parameters. Similarly, for three optimal thresholds 9 parameters, for four optimal thresholds 12 parameters will be required and so on. As the number of thresholds increases, the membership functions for each set will have to be updated accordingly.

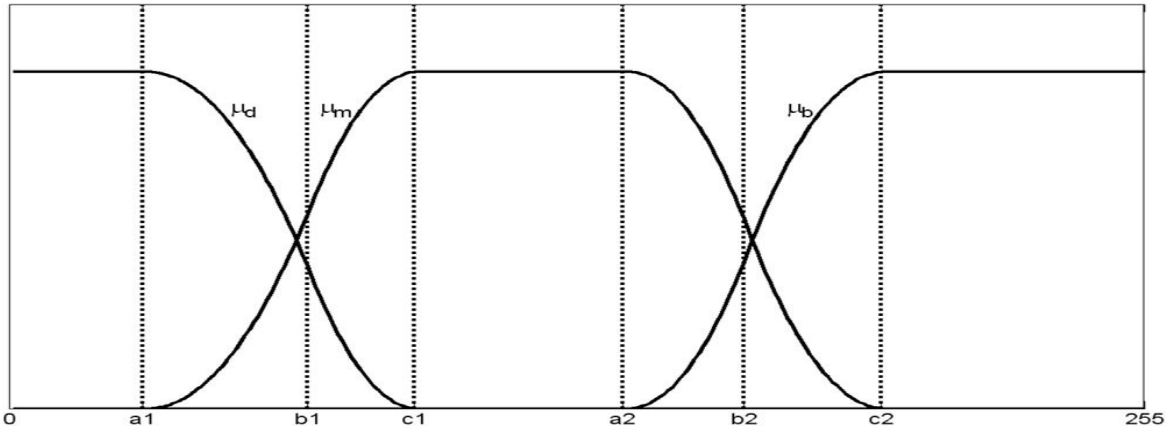

Fig 3.1 Membership function graph (Tao et al. 2007)

3.3 Basic Bat Algorithm (BA) adapted for Multilevel Image Thresholding

3.3.1 Echolocation behaviour of micro bats:

The Bat algorithm deals with the echolocation behavior of micro bats. To help them find prey in darkness, most bat species developed a remarkable sonar called echolocation. They emit extremely high pitch sound pulses and receive the echo that bounces back from the surrounding objects. By determining how long it takes a noise to return, the bats figure out how far the object/prey is. Micro bats can avoid obstacles as thin as a human hair. The typical range of frequencies for most bat species are in the region between 25kHz and 100kHz, though some species can emit higher frequencies up to 150 kHz. Each ultrasonic burst may last typically 5 to 20 ms, and microbats emit about 10 to 20 such sound bursts every second. When hunting for prey, the rate of pulse emission can be sped up to about 200 pulses per second when they fly near their prey. The emitted pulse could be as loud as 110 dB, and they are in the ultrasonic region. The loudness also varies from the loudest when searching for prey and to a quieter base when homing towards the prey. Such echolocation behaviour of microbats can be formulated in such a way that it can be associated with the objective function to be optimized [1].

3.3.2 Assumptions:

Some basic approximate or idealized rules have been developed for simplicity of application of this algorithm as defined by [1].

1. All bats use echolocation to sense distance, and they also 'know' the difference between food/prey and background barriers in some magical way;

2. Bats fly randomly with velocity v_i at position x_i with a fixed frequency f_{min}, varying wavelength λ and loudness A_0 to search for prey. They can automatically adjust the wavelength (or frequency) of their emitted pulses and adjust the rate of pulse emission $r \in [0,1]$,depending on the proximity of their target;

3. Although the loudness can vary in many ways, it is assumed that the loudness varies from a large (positive) A_0 to a minimum constant value A_{min}.

In general, in most of the image thresholding applications it is supposed $f \in [0,2]$, $A \in [1,2]$ and $r \in [0,1]$. A_i=2 denotes maximum loudness while A_i=1 denotes the minimum loudness. Similarly, r_i=0 denotes no pulse emission at all and r_i=1 signifies maximum level of pulse emission indicating that the bat has just found its prey.

3.3.3 The Bat Algorithm:

The purpose of the bat algorithm is to maximize the fuzzy entropy based objective function given by (3.13) so as to give rise to k threshold values based on (3.15), according to which the images will be segmented into multiple levels. The details of the developed BA approach are given as follows:

Step 1 (generate initial population of solutions). The initial bat population of n bats (solutions) is generated randomly by a uniform random distribution. Initializing the bat population means initializing the position of each of the *n* bats. The position of each bat is *d*-dimensional where *d* denotes the dimension of the search space. So, $b_{i,j}$ denotes the j^{th} dimension in the position vector of the i^{th} bat. The value of $b_{i,j}$ is restricted to $\{0, 1, \ldots, L-1\}$,where, $L= 2^8=256$, and $b_{i,j} < b_{i,j+1}$ holds for all j. Thus the initial solution is a *nxd* matrix B which can be represented as:

$$B = \begin{bmatrix} b_{1,1} & b_{1,2} & b_{1,3} & \ldots. & b_{1,d} \\ b_{2,1} & b_{2,2} & b_{2,3} & \ldots. & b_{2,d} \\ & & & & \vdots \\ b_{n,1} & b_{n,2} & b_{n,3} & \ldots. & b_{n,d} \end{bmatrix} \quad (3.16)$$

Out of these n random solutions, the bat algorithm finds the solution b_{best} which maximizes the fitness function and then the iterative search process starts. In this initialization step, the pulse rate r_i of each bat is also initialized randomly usually in the range [0,1] and the loudness of each bat A_i is initialized randomly in the range [1,2].

Step 2 (calculation of new solutions). By movement of the virtual bats new solutions are generated in each iteration. The current iteration is denoted by time instant *t*. The virtual bats are moved according to the equation

$$b_i^t = b_i^{t-1} + v_i^t, \tag{3.17}$$

where v_i^t denotes the velocity of bat movement and it is given by the expression

$$v_i^t = v_i^{t-1} + (b_i^{t-1} - b_{best}) * f_i\,, \tag{3.18}$$

v_i is initialized as a null vector, f_i denotes the frequency of the i[th] bat, and b_{best} is the current global best solution. f_i is given by the equation

$$f_i = f_{min} + (f_{max} - f_{min}) * \beta, \tag{3.19}$$

where $\beta \in [0,1]$ is a random vector drawn from the uniform random distribution. The recommended values $f_{max} = 2$, $f_{min} = 0$ have been chosen.

Step 3 (improving the current best solution). For each current solution b_i^t the following random walk step is performed.

$$b_{i,new}^t = \begin{cases} b_{best} + \ \in A^t, \ rand_1 > r_i \\ b_i^t, \ \ otherwise, \end{cases} \tag{3.20}$$

where $rand_1$ is a uniform random number in range [0,1], r_i is the pulse rate emitted by the i[th] bat, $\in$ is also another random number within [-1,1] and $A^t = \langle A_i^t \rangle$ is the average loudness of all bats at this time step. If after movement of the bats the value of the b_i^t vector overflows the permissible bounds, a computational step is incorporated which clips the values and brings them within the defined boundary.

Step 4 (accepting new solution). The solution $b_{i,new}^t$ obtained from Step 3 is accepted as the new solution and $f(b_{i,new}^t)$ is accepted as the new fitness value subject to the following condition

$$(b_i^t, f(b_i^t)) = \begin{cases} \left(b_{i,new}^t, f\left(b_{i,new}^t\right)\right), \\ if\ ((\ rand_2 < A_i)\ and\ f\left(b_{i,new}^t\right) > f(b_i^{t-1})) \\ (b_i^{t-1}, f(b_i^{t-1})), \quad otherwise \end{cases} \tag{3.21}$$

where $rand_2$ is a uniform random number in the range [0,1].

After this computation A_i is decreased and r_i is increased following the formula

$$A_i^{t+1} = \alpha A_i^t \tag{3.22}$$

$$r_i^{t+1} = r_i^0(1-e^{-\gamma t}) \tag{3.23}$$

where α and γ are constants and free parameters. r_i^0 is the initial pulse rate value of the i^{th} bat.

$$A_i^t \to 0,\ r_i^t \to r_i^0, \text{ as } t \to \infty.$$

This is the mathematical modelling of the natural phenomenon that when a bat nears towards a prey its loudness value decreases while its pulse emission rate increases. α is similar to the cooling factor of a cooling schedule in simulated annealing algorithm. Generally α is set equal to γ in the range [0,1] and initialized at the beginning of algorithm execution.

Step 5 (memorizing best solution so far).

$$\text{If } f(b_{i,new}^t) > f(b_{best})$$

$$b_{best} = b_{i,new}^t \text{ and } f(b_{best}) = f(b_{i,new}^t) \tag{3.24}$$

The best solution so far is recorded.

Step 6 (check stopping criteria). If the termination criterion is met or the maximum number of iterations is reached, then the algorithm is terminated. Otherwise increase the iteration number by 1 and repeat from step 2 to step 6.

3.3.4 Pseudo code of basic bat algorithm (BA):

Objective function f(b), $b = (b_1, b_2, \ldots, b_d)$

Initialize bat population $b_i = (i=1, 2, \ldots, n)$ and v_i

Define pulse frequency f_i at b_i

Set values for α and γ

Initialize pulse rate r_i and loudness A_i

while *(t < Max number of iterations)*

Generate new solutions by adjusting frequency, and updating velocities

and locations/solutions [equations (3.17) to (3.19)]

if *(rand > r_i)*

Select a solution among the best solutions

Generate a local solution around the selected best solution

end if

Generate a new solution by flying randomly

if *(rand < A_i & $f(b_i) > f(b_{best})$)*

Accept the new solutions

Increase r_i and reduce A_i

end if

Rank the bats and find the current best b_{best}

end while

Postprocess results and visualization

The key features that make the bat algorithm successful and advantageous over other metaheuristic algorithms are [14]:

- Frequency tuning: BA uses echolocation and frequency tuning to solve optimization problems. This frequency tuning parameter is similar to the key feature of particle swarm optimization (PSO) and contributes to the exploration.
- Automatic zooming: BA has the capability of automatically zooming into a region where a promising solution has been found. This exploitation is done by local random walk similar to one of the key features of harmony search optimization (HS). Hence speed of convergence increases.
- Parameter control: In general, metaheuristic algorithms use fixed, pre-tuned algorithm dependent parameters. But in BA, as the iteration progresses the control parameters A_i and r_i adjust their values and the algorithm intelligently switches from exploration to exploitation. This enhances the efficiency of the BA.

Thus BA possesses the advantages of other swarm-intelligence based metaheuristic algorithms.

3.4 Proposed Modified Hybridized Bat Algorithm (MHBA)

3.4.1 Background behind improvement of BA:

Although it has already been mentioned in the previous section the advantages that make the basic bat algorithm a very good choice for solving various optimization problems, but as the complexity of the problem increases, the BA starts losing its brilliance. In the present case of selecting optimal thresholds for multilevel MRI segmentation, as the number of thresholds increases, especially for the fuzzy entropy objective function, BA often fails. The solutions then tend to get trapped near the local maximum as the exploration capability of basic BA falls short for such complex situations dealing with the search space having a very large dimension. Hence, in order to improve the exploration capability of the BA, some features from the differential evolution (DE) algorithm [18], such as the concepts of mutation and crossover are included. Moreover, as suggested by [5], the concept of scout bees taken from the artificial bee colony (ABC) optimization algorithm [15] has also been incorporated. In addition to that, in order to mimic the bat's echolocation behaviour more intricately, the impact of Doppler Effect in echoes [7] which was previously ignored in the basic BA has also been considered. By incorporating all these special features in our proposed MHBA algorithm, there has been an attempt to achieve a good balance between intensification and diversification strategies, thus making the algorithm more efficient.

3.4.2 Doppler Effect in MHBA:

The Doppler Effect is the change in frequency of a wave for an observer moving relative to its source. Given the Doppler Effect, the perceived sound frequency can change due to the relative motion between the observer and the source. Let us suppose f_s and f_r are the frequencies of the source and the receiver, respectively; and v_r and v_s are the speeds of the receiver and the source, respectively. λ_0 is the wavelength, and v is the wave speed in the medium. Assuming moving source and moving receiver, the f_r can be formulated as follows:

$$f_r = \frac{v \pm v_r}{v \mp v_s} f_s \tag{3.25}$$

The - and + signs for the values substituted for v_r and v_s depend on the direction of the velocity. + is used for the relative motion of the receiver or the source toward the other, and – for the relative motion of one away from the other. In conclusion, the perceived source frequency is decreased if either is moving away from the other, and increased if either is moving toward the other.

Given the Doppler Effect, the formula for updating $b_{i,j}^t$ and $v_{i,j}^t$ at time step t are slightly different from the corresponding parts in original BA, and is done according to (3.26), (3.27), (3.28) and (3.29) respectively. Apart from assigning a frequency randomly chosen from the interval f_{min} to f_{max}, the frequency also depends on the Doppler Effect and the bat's compensation rate C_i for Doppler Effect. Since the objective of the bats is to catch the prey, + sign should be adopted in (3.25). Here, the global best solution $b_{best,j}$ may be regarded as the prey. The bats may positively compensate for the Doppler Effect in echoes and fly forwards to catch the prey when $b_{best,j}$ is greater than $b_{i,j}$ at the t^{th} time instant. If $b_{best,j}$ is smaller than $b_{i,j}$, the bats may negatively compensate for the Doppler effect in echoes and slows down to capture its prey. The compensation rate varies with individual bats.

3.4.3 Crossover, Mutation and Scout technique in MHBA:

For an algorithm to be efficient and effective, it must be able to generate a diverse range of solutions including the potentially optimal solutions so as to explore the whole search space effectively, while it intensifies its search around the neighbourhood of an optimal or nearly optimal solution. As the dimension of the search space increases as it is with our case of fuzzy entropy based multilevel image thresholding, the basic BA often fails to produce optimal results since it lacks in effective diversification. In order to enhance this diversification ability of the BA, the concepts of crossover and mutation from DE algorithm [5] which essentially have the essence of randomization, have been incorporated. Mutation and crossover is the process by which DE generates new vectors by adding the weighted difference between two population vectors to a third vector. As shown in (3.31), F is the differential weight which is a real constant factor and $\in[0,2]$, $C_r \in[0,1]$ is the constant crossover probability and these value is fixed by the user. So it is seen that during the beginning of the iteration as r_i^t is of small value, mutation and crossover operator is highly predominant and results in effective diversification. As the number of iterations increase, intensification enhances and the algorithm approaches towards getting optimal solutions.

Moreover, some solutions may still be there which have a tendency to get stuck in some local optimum. In order to fix this, the launch of scout phase of the ABC algorithm has been introduced. When a solution refuses to improve after a fixed number of consecutive iterations, it will eventually exceed the predetermined number of allowed trials called *limit.* Then that particular solution is again initialized randomly.

3.4.4 Proposed Modified Hybridized Bat Algorithm (MHBA):

Step 1 (generate initial population of solutions). Similar to basic BA, our proposed MHBA first randomly generates n bat populations of d-dimensions and matrix (3.16) is created. So, $b_{i,j}$ denotes the jth dimension in the position vector of the ith bat. The value of $b_{i,j}$ is restricted to {0, 1, …, *L*-1} ,where, $L= 2^8=256$, and $b_{i,j} < b_{i,j+1}$ holds for all j. Apart from initializing A_i and r_i, the parameter *limit* which presents the number of allowed attempts to improve a bat is also initialized. The parameters in the differential evolution (DE) algorithm such as the differential weight *F* and crossover probability C_r are also initialized. Out of these n random solutions, the bat algorithm finds the solution b_{best} which maximizes the fitness function and then the iterative search process starts.

Step 2 (calculation of new solutions considering Doppler effect in echoes). Considering the Doppler effect [7], the formula of updating the current solution in each iteration slightly differs from that of basic BA. An additional parameter *w* called inertia weight is incorporated to update velocity. It controls to what degree the previous velocity of an individual is inherited. The current iteration is denoted by time instant t. Mathematically; the process of updating is done as follows:

$$f_{i,j} = f_{min} + (f_{max} - f_{min}) * \beta, \tag{3.26}$$

$$f_{i,j} = \frac{(c+v_{i,j}^{t-1})}{(c+v_{best,j}^{t-1})} * f_{i,j} * (1 + C_i * \frac{\left(b_{best,j} - b_{i,j}^{t-1}\right)}{|b_{best,j} - b_{i,j}^{t-1}| + \varepsilon}), \tag{3.27}$$

$$v_{i,j}^{t} = w * v_{i,j}^{t-1} + \left(b_{best,j} - b_{i,j}^{t-1}\right) * f_{i,j}\ , \tag{3.28}$$

$$b_{i,j}^{t} = b_{i,j}^{t-1} + v_i^t, \tag{3.29}$$

where, $w \in [0,1]$ and $\beta \in [0,1]$ are uniform random vectors. $f_{max} = 2$ and $f_{min} = 0$ similar to basic BA. ε is the smallest possible constant available in the computer, it avoids zero-division-error. C_i is a positive number randomly chosen in the interval [0,1]. 0 means the bat cannot compensate for Doppler effect in echoes, while 1 means the bat can fully compensate for it. *c* is the speed of sound in air (c = 340m/s), $v_{best,j}$ is the velocity corresponding to the global best position.

Step 3 (improving the current best solution by differential operators). For each solution b_i^t, the following operator given (3.30) has been applied

$$b_{new} = \begin{cases} b_{diff}^t, & if\ rand_1 > r_i^t \\ b_{loc}^t, & otherwise, \end{cases} \tag{3.30}$$

where $rand_1$ is randomization term in the range [0, 1], r_i^t is the pulse rate function defined by (3.23), b^t_{diff} is the differential operator for mutation and crossover, and b^t_{loc} is the operator based on the local search in the BA. The differential mutation and crossover operations are performed by

$$b_{dif,j}^t = \begin{cases} b_{c,j}^t + F\left(b_{a,j}^t - b_{b,j}^t\right) & if\ (rand_2 < C_r\ or\ j = j_r) \\ b_{i,j}^t & otherwise, \end{cases} \tag{3.31}$$

where *F* is the differential weight which scales the rate of modification, C_r is the crossover probability and $rand_2$ is a uniform random number drawn from the interval [0,1]. j_r is randomly selected from the interval [1,*d*] where *d* is the dimension of the search space; b_a, b_b and b_c are three randomly chosen bats (solutions) out of the *n* prospective solutions at the cycle *t*, such that a≠b≠c≠i. Here, the "DE/rand/1/bin" scheme pertaining to the DE algorithm [18] has been used. Normally, *F* is chosen in the range 0.4 to 1.0, and C_r is chosen close to 1 to increase the speed of convergence [18]. In this thesis work, F=0.5 and C_r=0.9 has been chosen.

This step ensures proper diversification during initial stages and then as the number of iterations increases, proper intensification is ensured. Thus a proper balance of intensification and diversification is obtained and the efficiency of the algorithm is enhanced. The local search is performed by

$$b_{loc,j}^{t} = \begin{cases} b_{lbest,j}^{t} & if(f(b_{lbest,j}^{t}) > f(b_{i,j}^{t})) \\ b_{i,j}^{t} & otherwise, \end{cases} \quad (3.32)$$

where, $b_{lbest,j}^{t} = b_{best,j}^{t-1} + \epsilon A^{t}$ (3.33)

Just like basic BA, $\in$ is uniform random number in the range [-1,1] and $A^t = \langle A_{i,j}{}^t \rangle$ is the average loudness of all bats at this time step. At the end of step 3, the boundary conditions for all j (j=1, 2... *d*) are checked and an overflow, if any, is suitably adjusted.

Step 4 (accepting new solution). After completion of step 3, the new solutions generated so far are accepted base on

$$\left(b_i^t, fit(b_i^t)\right) = \begin{cases} \left(b_{new}^t, f(b_{new}^t)\right) & if\ (rand_3 < A_i^t\ and\ f(b_{new}^t) > f(b_i^{t-1})) \\ \left(b_i^{t-1}, f(b_i^{t-1})\right) & ,\ \ tr_i = tr_i + 1, \qquad otherwise \end{cases} \quad (3.34)$$

where $rand_3$ is a uniform random number from [0,1] and tr_i is the *trial* array of size 1x*n* which records the number of attempts through which a given solution $b_i{}^t$ could not improve. The incorporation of the *trial* array is inspired by the launch of scouts in the scout phase of ABC algorithm. Every time a particular ith solution cannot improve in a subsequent iteration, tr_i increases by 1 as shown in (3.34). Also, after a certain continuous number of cycles determined by the *limit*, if the solution cannot be improved further, it is abandoned and replaced by a randomly generated solution. The value of *limit* has been chosen to be 150. Subsequently, the ith element of the trial vector is set to 0. This modification prevents the solution from getting trapped in a local maximum, as well as improves the exploration process. Moreover, if the solution is improved, A_i^t is decreased and $r^t{}_i$ is increased following the formulas (3.22) and (3.23) respectively.

Step 5 (memorizing best solution so far). The best solution, so far obtained is memorized in a similar fashion as basic BA, according to (3.24).

Step 6 (check stopping criteria). If the termination criterion is met or the maximum number of iterations is reached, then the algorithm is terminated. Otherwise increase the iteration number by 1 and repeat from step 2 to step 6.

3.4.5 Pseudocode of MHBA:

Input**:** *n: Number of individuals (bats) contained by the population.*

d: Dimension of search space.

N_gen: Maximum number of iterations.

C_r: Crossover probability.

F: Differential weight.

limit: Trial limit.

w: Inertia weight.

c: Speed of sound in air.

C: Compensation rate for Doppler effect in echoes.

f_{min}, f_{max}, α, γ, A_{min}, A_{max}, r_{min}, r_{max},: Parameters in basic BA.

t=0; Initialize the population and the related parameters.

Evaluate objective function for each bat using (3.13).

Find the best solution.

While*(t< N_gen)*

For *i= 1 to n*

Generate new solutions using (3.26) to (3.29).

If*(rand(0,1)> r_i)*

For *j= 1 to d*

If*(rand(0,1) ≤ C_r || j== randi[1,d])*

Perform mutation and crossover using (3.31)

End If

End For

Else

Perform local random walk using (3.33)

End If Else

Evaluate the objective function of each individual solution using (3.13)

Accept solutions using (3.34)

Decrease A_i using (3.22)

Increase r_i using (3.23)

If *$tr_i \geq limit$*

Abandon i^{th} solution and replace by a random solution, satisfying constraints

End If

Update global best solution using (3.24)

End For

t=t+1;

End while

Output: *The individual with best objective value in population.*

3.5 Results and Discussions:

Our purpose is to perform efficient brain MRI segmentation using the proposed MHBA algorithm and compare the results with the basic BA. The real-patient MRI Multiple sclerosis database (MRI MS DB) obtained from Institute of Neurology and Genetics, Nicosia, Cyprus has been downloaded to be used as the database of the present work. The transverse T2-weighted MR images were obtained using a 1.5T whole body Philips ACS NT MR imager [57-60]. Each image has 8-bit representation and is of size 512x512. Hence there are $L= 2^8= 256$ gray levels in each image and its corresponding histogram. The MR images have been initially pre-processed to remove any unwanted image artifacts and noise. Then the proposed MHBA algorithm has been applied to 10 pre-processed MRI slices and the segmentation results have been compared with those obtained from applying the basic BA.

The work has been implemented by the language of Matlab® 2015a on a personal computer with a 3.8 Ghz CPU, 4.00GB RAM under 32-bit Windows 7 operating system.

3.5.1 Parameter Setting:

Parameter	Meaning	Values
n	Number of bats in the population	50
N_gen	Number of iterations	1000
f_i	Frequency of each bat	[0,2]
r_i	Rate of pulse emission of each bat	[0,1]
A_i	Loudness of each bat	[1,2]
α	Loudness decrement constant	0.9
γ	Pulse rate increment constant	0.9

Table 1: Parameters used in basic BA.

Parameter	Meaning	Values
n	Number of bats in the population	50
N_gen	Number of iterations	1000
f_i	Frequency of each bat	[0,2]
r_i	Rate of pulse emission of each bat	[0,1]
A_i	Loudness of each bat	[1,2]
α	Loudness decrement constant	0.9
γ	Pulse rate increment constant	0.9
C_r	Crossover probability	0.9
F	Differential weight	0.5
limit	Trial limit	150
w	Inertia weight	[0,1]
C	Compensation rate for Doppler effect in echoes of each bat	[0,1]

Table 2: Parameters used in proposed MHBA.

The number of thresholds (*k*) implemented in the experiments were 2, 3 and 4. Since metaheuristic algorithms have stochastic characteristics, each experiment was repeated 30 times for each image and each threshold and the average solution was considered. For one run of each image and each threshold, the total number of objective function evaluation is *n* x *N_gen*= 50000. One of the major challenges for satisfactory performance of metaheuristic algorithms is the choice of its numerous free parameters. In the present work, parameters as shown in Table 1 and Table 2 for BA and MHBA respectively, have been selected based on trial and error, and also based on some prior knowledge [5,7].

3.5.2 Qualitative and Quantitative Analysis:

MRI Slice Number	*K*	Basic BA Threshold values	Proposed MHBA Threshold values
09	2	[116 , 180]	[92 , 182]
	3	[109 , 151 , 218]	[64 , 132 , 202]
	4	[86 , 126 , 168 , 225]	[70 , 120 , 164, 214]
10	2	[118 , 185]	[97 , 179]
	3	[109 , 151 , 208]	[62 , 124 , 197]
	4	[88 , 131 , 172 , 227]	[48 , 99 , 153 , 211]
11	2	[121 , 200]	[91 , 168]
	3	[108 , 149 , 217]	[71 , 130 , 206]
	4	[94 , 133 , 172 , 222]	[56 , 107 , 157 , 215]
12	2	[124 , 190]	[98 , 181]
	3	[113 , 157 , 218]	[63 , 133 , 201]
	4	[91 , 134 , 172 , 225]	[54 , 112 , 160 , 218]
13	2	[120 , 186]	[103 , 186]
	3	[110 , 155 , 219]	[67 , 130 , 200]
	4	[91 , 136 , 174 , 219]	[55 , 107 , 161 , 213]
14	2	[122 , 183]	[97 , 179]
	3	[105 , 146 , 205]	[68 , 130 , 197]
	4	[89 , 132 , 170 , 209]	[43 , 96 , 148 , 212]
15	2	[123 , 212]	[107 , 186]
	3	[107 , 146 , 220]	[68 , 133 , 200]
	4	[89 , 131 , 170 , 225]	[53 , 107 , 165 , 221]
16	2	[119 , 210]	[79 , 188]
	3	[107 , 152 , 221]	[65 , 133 , 211]
	4	[85 , 125 , 168 , 224]	[52 , 100 , 160 , 218]
17	2	[121 , 201]	[91 , 185]
	3	[107 , 152 , 215]	[76 , 141 , 210]
	4	[77 , 118 , 168 , 216]	[44 , 105 , 163 , 214]
18	2	[119 , 205]	[101, 195]
	3	[107 , 151 , 220]	[64 , 140 , 211]
	4	[74 , 126 , 158 , 218]	[38 , 103 , 152 , 217]

Table 3: Threshold values in BA and MHBA.

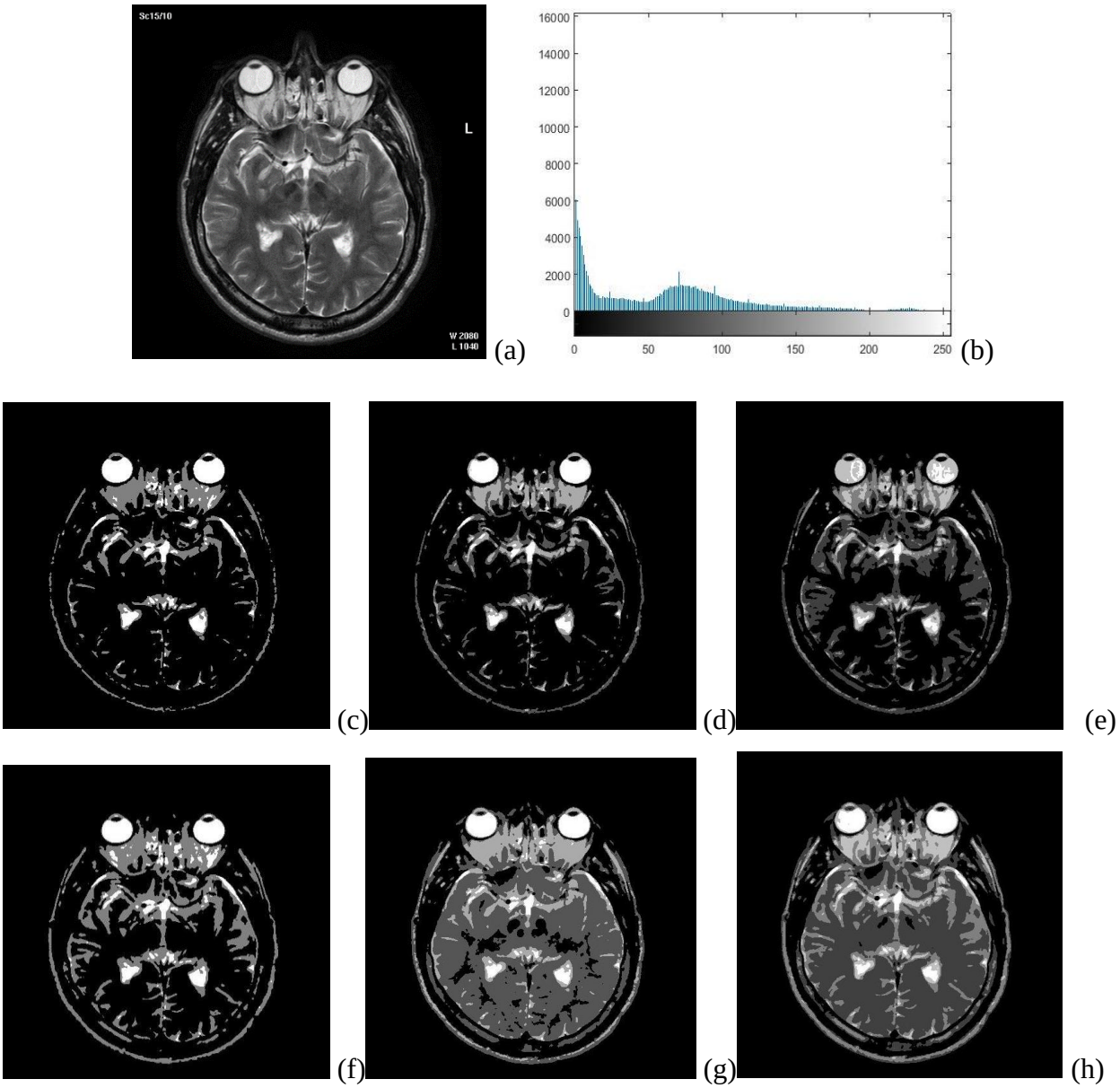

Fig 3.2 (a) Original image for slice #10, (b) Histogram for slice #10

(c) Segmented image using BA for *k*=2, (d) Segmented image using BA for *k*=3

(e) Segmented image using BA for *k*=4, (f) Segmented image using MHBA for *k*=2

(g) Segmented image using MHBA for *k*=3, (h) Segmented image using MHBA for *k*=4

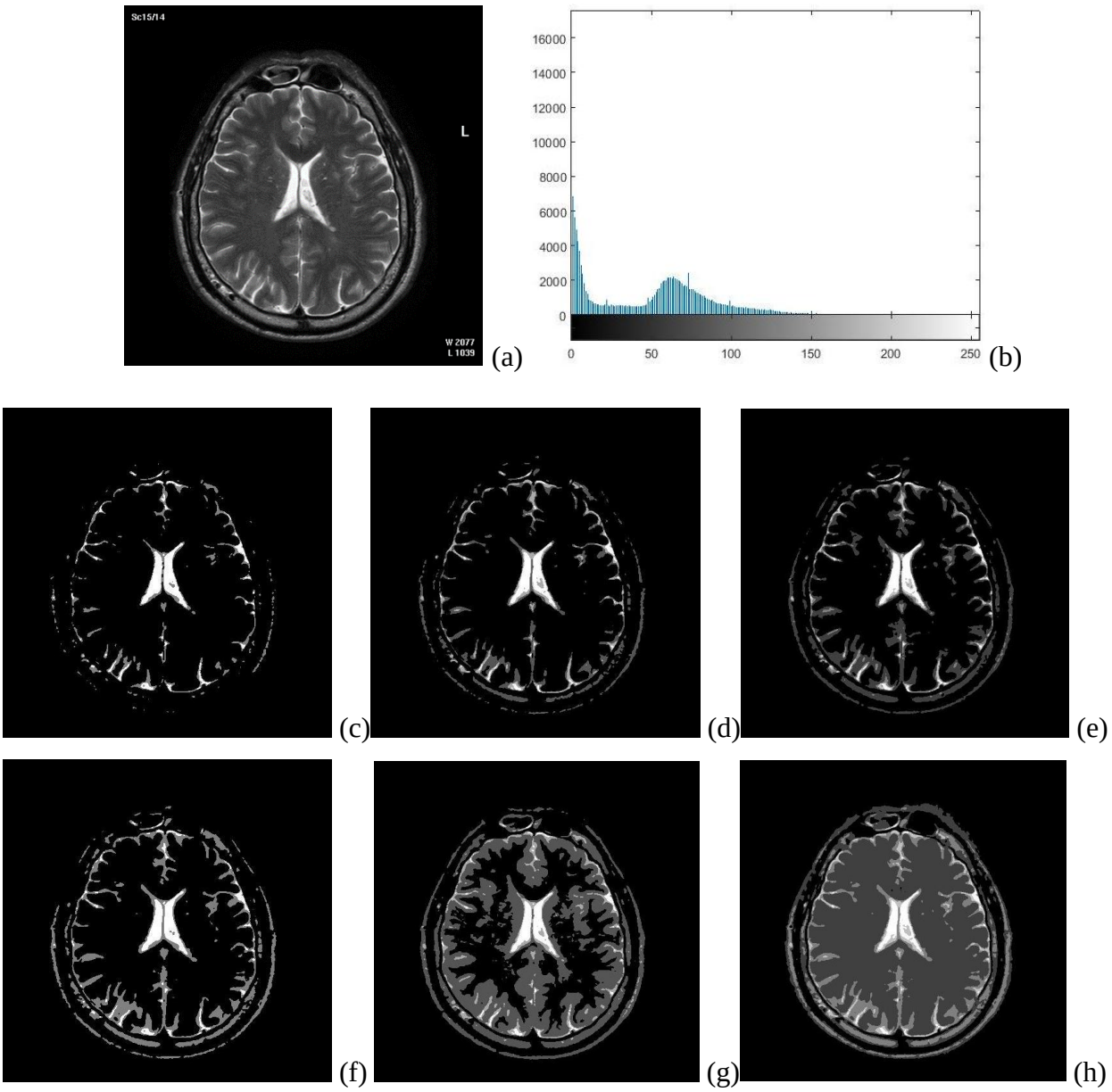

Fig 3.3 (a) Original image for slice #14, (b) Histogram for slice #14

(c) Segmented image using BA for *k*=2, (d) Segmented image using BA for *k*=3

(e) Segmented image using BA for *k*=4, (f) Segmented image using MHBA for *k*=2

(g) Segmented image using MHBA for *k*=3, (h) Segmented image using MHBA for *k*=4

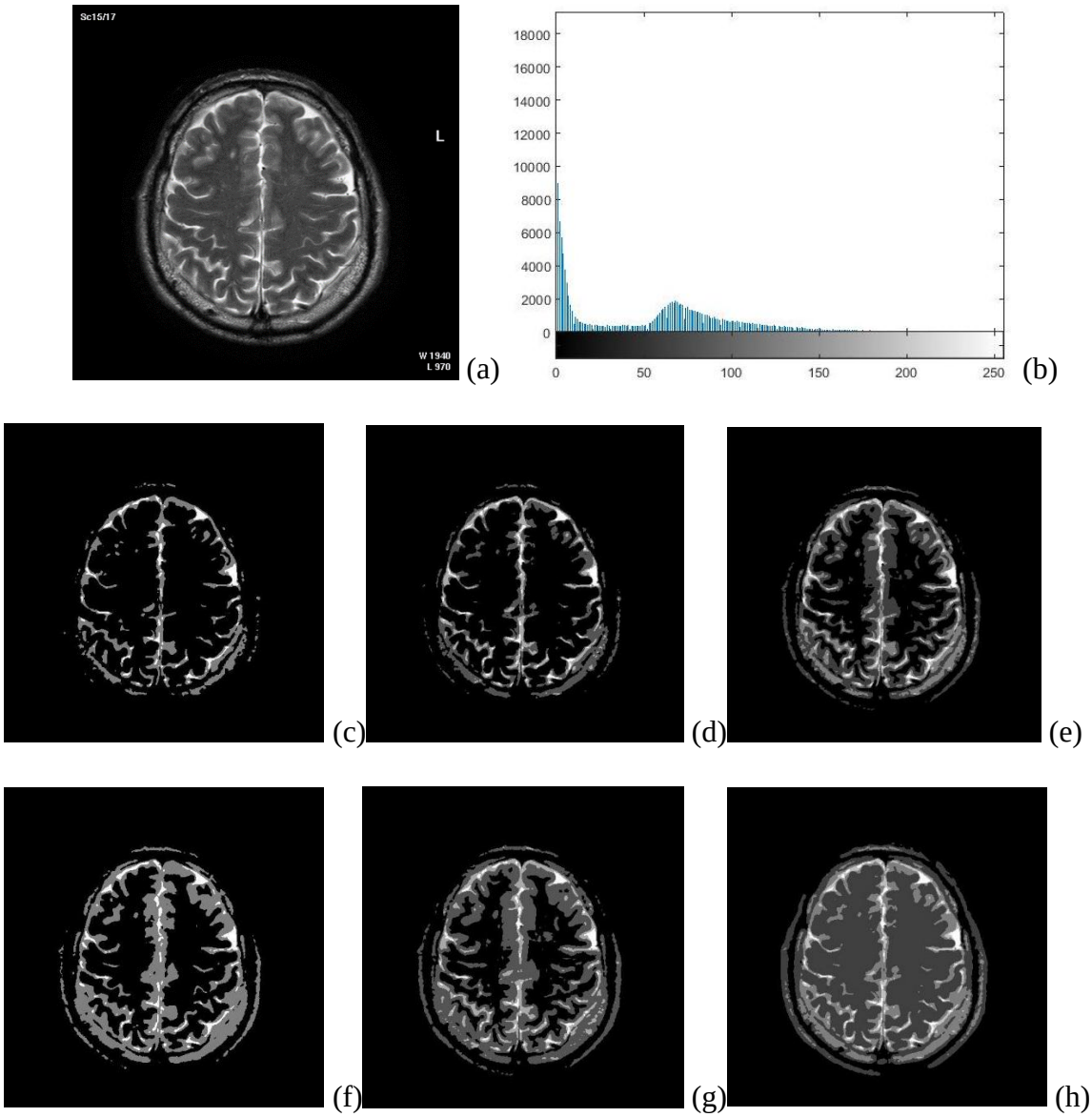

Fig 3.4(a) Original image for slice #17, (b) Histogram for slice #17

(c) Segmented image using BA for *k*=2, (d) Segmented image using BA for *k*=3

(e) Segmented image using BA for *k*=4, (f) Segmented image using MHBA for *k*=2

(g) Segmented image using MHBA for *k*=3, (h) Segmented image using MHBA for *k*=4

In order to quantitatively judge the quality of thresholding-based segmentation algorithms a validity function called the uniformity factor has been employed, which has been extensively used in several literatures [20,30]. This uniformity factor is given as

$$V_u = 1 - 2 * k * \frac{\sum_{j=0}^{k} \sum_{i \in R_j} (I_i - \mu_j)^2}{N * (I_{max} - I_{min})^2} \quad (3.35)$$

where,

k → Number of thresholds,

R_j → j[th] segmented region,

N → Total number of pixels in the given image,

I_i → Gray level of pixel i,

μ_j → Mean gray level of pixels in the j[th] region,

I_{max} → Maximum gray level of pixels in the given image,

I_{min} → Minimum gray level of pixels in the given image.

The value of V_u should be a positive fraction in the range [0,1]. A higher value of V_u conveys a high level of uniformity among the pixels of each segment of the image, thus depicting a better quality of thresholding. Conversely, a lower value of V_u means a worse quality of thresholding.

MRI Slice No.	*K*	Mean Entropy		Maximum Entropy		Minimum Entropy		St. Dev of Entropy		Uniformity (V_u)	
		BA	MHBA	BA	MHBA	BA	MHBA	BA	MHBA	BA	MHBA
09	2	**11.866**	11.861	11.873	11.873	11.806	**11.822**	**0.017**	0.020	0.9796	**0.9830**
	3	15.497	**15.526**	15.564	15.564	15.351	**15.458**	0.047	**0.028**	0.9726	**0.9865**
	4	18.675	**18.709**	18.773	**18.775**	18.090	**18.263**	0.162	**0.122**	0.9767	**0.9841**
10	2	**11.798**	11.788	**11.809**	11.808	11.698	**11.738**	**0.030**	0.031	0.9795	**0.9832**
	3	15.346	**15.410**	15.440	**15.455**	15.165	**15.296**	0.068	**0.037**	0.9748	**0.9875**
	4	18.564	**18.570**	18.660	**18.661**	**18.167**	18.068	**0.142**	0.153	0.9773	**0.9902**
11	2	**11.947**	11.795	**11.967**	11.809	**11.891**	11.738	**0.022**	0.026	0.9801	**0.9846**
	3	15.631	**15.668**	**15.703**	15.692	15.503	**15.568**	0.058	**0.028**	0.9761	**0.9859**
	4	18.838	**18.880**	18.926	**18.935**	**18.596**	18.275	**0.087**	0.120	0.9757	**0.9893**

MRI Slice No.	*K*	Mean Entropy		Maximum Entropy		Minimum Entropy		St. Dev of Entropy		Uniformity (V_u)	
		BA	MHBA	BA	MHBA	BA	MHBA	BA	MHBA	BA	MHBA
12	2	11.859	**11.870**	11.878	11.878	11.805	**11.855**	0.028	**0.0094**	0.9804	**0.9858**
	3	**15.617**	15.584	15.638	15.638	15.432	**15.525**	0.061	**0.030**	0.9755	**0.9867**
	4	18.753	**18.760**	18.843	18.843	18.138	**18.142**	**0.128**	0.1646	0.9791	**0.9883**
13	2	11.897	**11.912**	11.920	11.920	11.810	**11.835**	0.041	**0.021**	0.9807	**0.9844**
	3	15.618	**15.643**	15.660	**15.664**	15.543	**15.591**	0.045	**0.021**	0.9755	**0.9868**
	4	18.855	**18.887**	18.949	**18.957**	18.677	**18.817**	0.066	**0.047**	0.9772	**0.9891**
14	2	11.865	**11.866**	11.867	11.867	11.864	**11.865**	0.001	0.001	0.9829	**0.9875**
	3	15.605	**15.636**	15.654	**15.656**	15.508	**15.608**	0.042	**0.016**	0.9808	**0.9877**
	4	18.926	**18.945**	18.990	**18.992**	18.685	**18.857**	0.069	**0.0457**	0.9809	**0.9916**
15	2	11.720	**11.738**	11.743	11.743	11.649	**11.681**	0.028	**0.015**	0.9830	**0.9866**
	3	15.442	**15.466**	15.495	**15.496**	15.278	**15.445**	0.056	**0.012**	0.9816	**0.9869**
	4	18.584	**18.587**	**18.712**	18.710	18.021	**18.022**	**0.176**	0.222	0.9825	**0.9917**
16	2	11.597	**11.611**	11.616	11.616	11.548	**11.5851**	0.019	**0.010**	0.9852	**0.9873**
	3	15.268	**15.304**	15.321	**15.322**	15.147	**15.260**	0.053	**0.014**	0.9832	**0.9875**
	4	18.433	**18.510**	18.587	**18.5890**	17.905	**17.949**	0.207	**0.153**	0.9850	**0.9917**
17	2	11.377	**11.385**	11.389	**11.389**	11.333	**11.379**	0.016	**0.004**	0.9874	**0.9890**
	3	15.047	**15.101**	15.118	**15.121**	14.940	**15.021**	0.058	**0.0183**	0.9864	**0.9894**
	4	18.137	**18.196**	18.338	**18.352**	18.816	**18.855**	**0.182**	0.216	0.9896	**0.9914**
18	2	11.203	**11.213**	11.215	**11.215**	11.148	**11.197**	0.014	**0.0051**	0.9887	**0.9906**
	3	14.935	**14.976**	14.987	14.987	14.762	**14.949**	0.067	**0.0105**	0.9877	**0.9882**
	4	**18.054**	17.985	18.178	**18.202**	17.770	**17.824**	0.138	**0.134**	0.9899	**0.9922**

Table 4: Comparison of mean entropy, maximum entropy, minimum entropy, standard deviation of entropy and uniformity between BA and MHBA for 30 runs each with *n*=50, *N_gen*=1000. (The better values are written in bold.)

Table 3 shows the different threshold values in both the cases of BA and MHBA. Table 4 shows the comparative performance of BA and proposed MHBA algorithms for threshold k = 2, 3 and 4. The comparison is carried on the basis of maximization of the mean objective function i.e, mean entropy of the solution, standard deviation between the entropies of 30 sets of solutions for each image and each threshold and, most importantly, the uniformity measure of each image obtained at the end of the segmentation process. It is observed that in majority of the images our proposed MHBA algorithm outweighs the performance of basic BA. Table 5 shows this quantitatively as

K	Name of parameter	% of images where MHBA performs better
2	Mean entropy	7/10 = 70%
	Std. Deviation of entropy	6/10 = 60%
	Uniformity	10/10 = 100%
3	Mean entropy	9/10 = 90%
	Std. Deviation of entropy	10/10 = 100%
	Uniformity	10/10 = 100%
4	Mean entropy	9/10 = 90%
	Std. Deviation of entropy	5/10 = 50%
	Uniformity	10/10 = 100%

Table 5: Performance of MHBA over 10 MRI slices.

Thus, it is seen that our proposed MHBA algorithm delivers better uniformity factor for all the images over all the thresholds 2, 3 and 4. Moreover, as the number of thresholds increases, the mean entropy increases and our proposed method has higher mean entropy in comparison to basic BA for each threshold.

Some representative MRI slices, along with their thresholding-based segmented versions (with k=2, k=3 and k=4) are displayed in Fig 3.2-3.4 for both BA and MHBA. These figures reveal that the proposed MHBA algorithm produces much smoother and more uniform segmentation for each threshold. Moreover, as the number of thresholds increases the proposed MHBA produces segmented images that resemble the original image more closely. The visual representation is in

conformation with the quantitative result shown in Table 4 with an exception to slice #18 where the MHBA uniformity reduces from 0.9906 for *k*=2 to 0.9882 for *k*=3 and again rises to 0.9922 for *k*=4, but the values are still higher than the respective uniformity values in the case of BA.

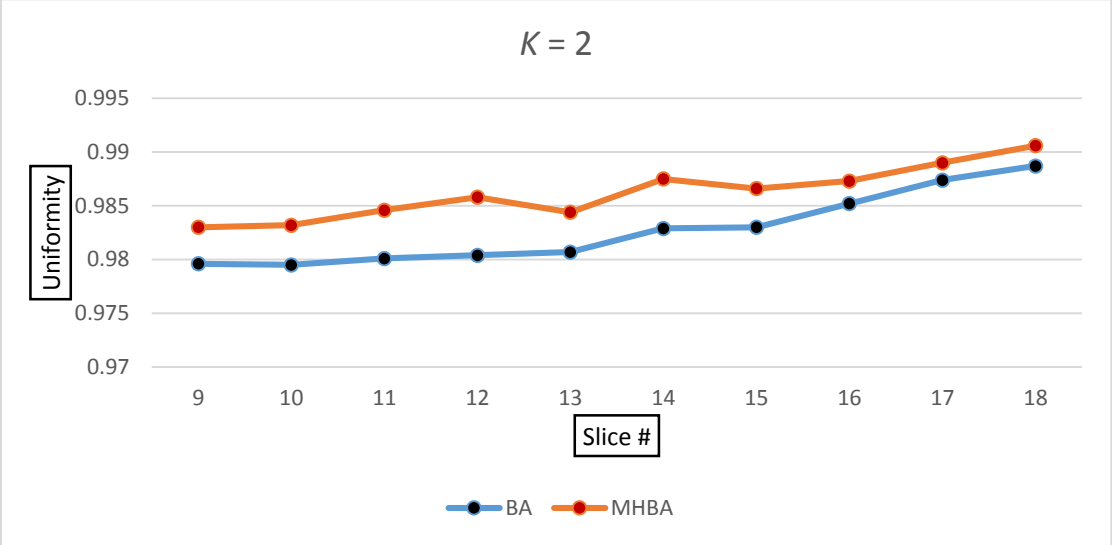

(a)

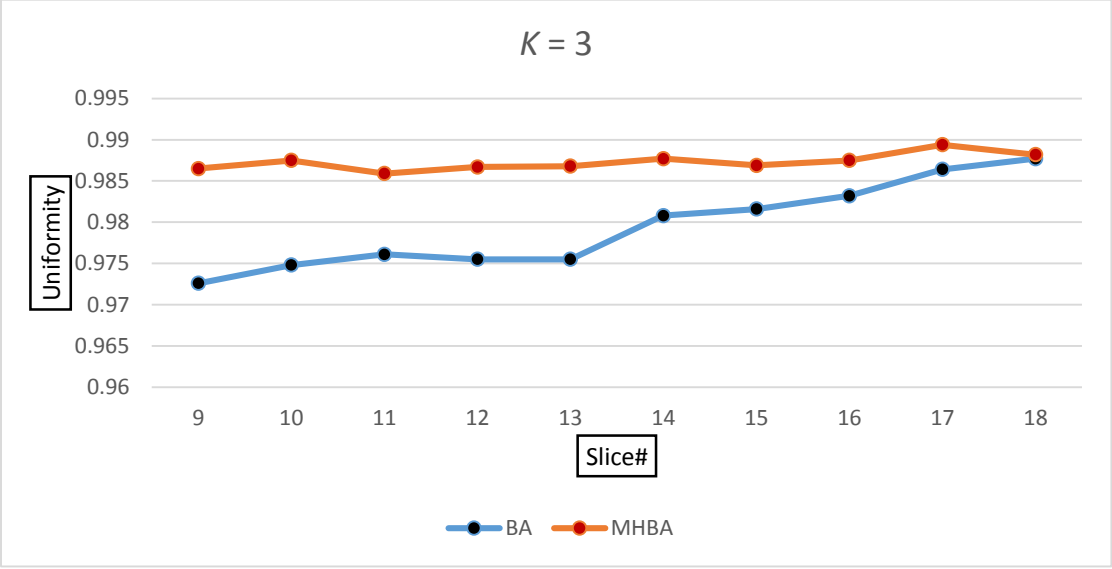

(b)

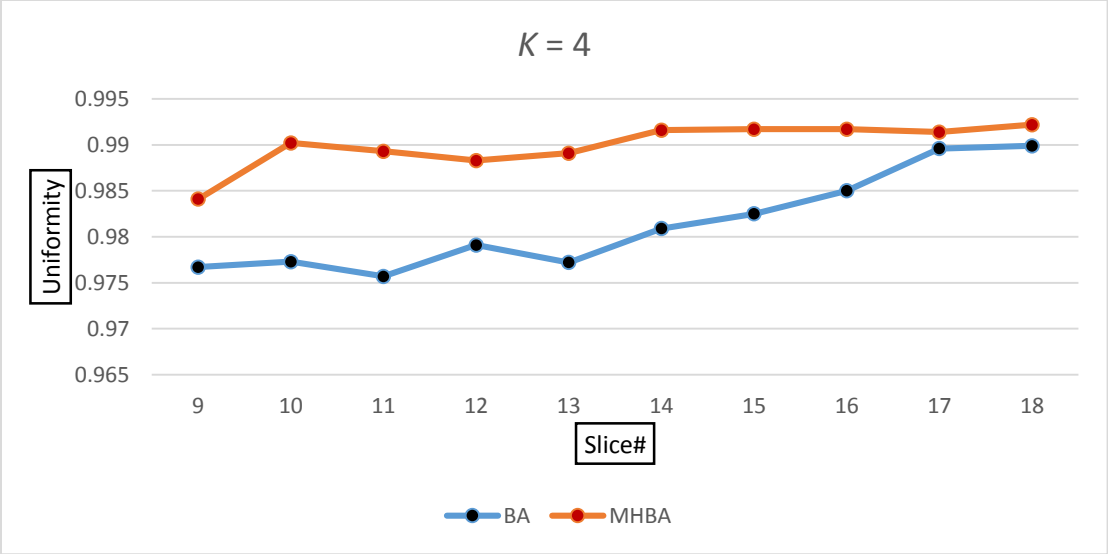

(c)

Fig 3.5 (a) Uniformity comparison for k=2, (b) Uniformity comparison for k=3
(c) Uniformity comparison for k=4

For ease of visualization, Fig 3.5 graphically depicts the variation of the uniformity factor V_u over the 10 MRI slices, in both the cases of basic BA and the proposed MHBA, for k=2, k=3 and k=4. Thus, one can easily conclude that the proposed MHBA algorithm has resulted in a more optimal thresholding of the said MR images in comparison to basic BA, and this is evident from the higher values of uniformity factor that have been obtained with MHBA for each of the 10 MRI slices under study.

3.6 Conclusions

In this chapter, a comparatively recent metaheuristic algorithm, called the Bat Algorithm (BA) has been studied for optimal multilevel thresholding-based segmentation of brain MR images, taking fuzzy entropy of image histogram as the objective function. It has been observed that the bat algorithm, in its basic version fails to give satisfactory segmentation results because of its tendency to get trapped in local optimum due to a lesser scope of exploration. Hence, in the present work, an attempt has been made to overcome these drawbacks by modifying the basic BA to form a Modified Hybridized Bat Algorithm (MHBA). MHBA has been developed by incorporating the concepts of mutation and crossover from Differential Evolution algorithm, which add to the

exploration capability of the bats and also by incorporating the concept of Doppler Effect in echoes, which aims to mimic the bat's echolocation behaviour more realistically. After application of both basic BA and proposed MHBA for multilevel thresholding of brain MRI, it has been observed that MHBA results in higher value of objective function for majority of the images. Moreover, MHBA produces smoother segmented images having higher uniformity factor in comparison to basic BA. All these facts lead to the conclusion that MHBA could achieve quite a substantial improvement over the basic BA in terms of maximizing an objective function (designed on the basis of an entropy based performance criterion) and also in terms of obtaining higher uniformity measure (used to quantitatively denote the quality of image segmentation).

References

[1] X.-S. Yang, "A New Metaheuristic Bat-Inspired Algorithm", in: Nature Inspired Co-operative Strategies for Optimization (NISCO 2010) (Eds. J. R. Gonzalez et al.), Studies in Computational Intelligence, Springer Berlin, 284, Springer, 65-74 (2010).

[2] Xin-She Yang and Amir H. Gandomi, "Bat Algorithm: A Novel Approach for Global Engineering Optimization, Engineering Computations", Vol. 29, Issue 5, pp. 464--483 (2012).

[3] Seyedali Mirjalili, Seyed Mohammad Mirjalili and Xin-She Yang, "Binary bat algorithm". Neural Comput & Applic (2014) 25:663–681 DOI 10.1007/s00521-013-1525-5.

[4] Md. Wasi Ul Kabir, Nazmus Sakib, Syed Mustafizur, and Mohammad Shaiful Alam, "A Novel Adaptive Bat Algorithm to Control Explorations and Exploitations for Continuous Optimization Problems". International Journal of Computer Applications (0975 – 8887), Volume 94 – No 13, May 2014

[5] Adis Alihodzic and Milan Tuba, "Improved Bat Algorithm Applied to Multilevel Image Thresholding". Hindawi Publishing Corporation, The Scientific World Journal, Volume 2014, Article ID 176718, 16 pages.

[6] Zhi-Wei Ye∗, Ming-Wei Wang, Wei Liu and Shao-Bin Chen, "Fuzzy entropy based optimal thresholding using bat algorithm", Applied Soft Computing 31 (2015) 381–395.

[7] Xian-Bing Meng, X.Z. Gao, Yu Liu and Hengzhen Zhang, "A novel bat algorithm with habitat selection and Doppler effect in echoes for optimization", Expert Systems with Applications 42 (2015) 6350–6364.

[8] Chiranjeevi Karri and Umaranjan Jena, "Fast vector quantization using a Bat algorithm for image compression", Engineering Science and Technology, an International Journal (2015).

[9] Eneko Osaba, Xin-She Yang, Fernando Diaz, Pedro Lopez-Garcia and Roberto Carballedo, "An improved discrete bat algorithm for symmetric and asymmetric Traveling Salesman Problems", Engineering Applications of Artificial Intelligence 48 (2016) 59–71.

[10] Ming-Liang Gao, Jin Shen, Li-Ju Yin, Wei Liu, Guo-Feng Zou, Hai-Tao Li and Gui-Xia Fu, "A novel visual tracking method using bat algorithm", Neurocomputing 177 (2016) 612–619.

[11] B.R. Adarsh, T. Raghunathan, T. Jayabarathi and Xin-She Yang, "Economic dispatch using chaotic bat algorithm". Energy 96 (2016) 666-675.

[12] Leandro dos, Santos Coelho and Alireza Askarzadeh, “An enhanced bat algorithm approach for reducing electrical power consumption of air conditioning systems based on differential operator”, Applied Thermal Engineering 99 (2016) 834‑840.

[13] Ali Osman Topal and Oguz Altun, “A novel meta-heuristic algorithm: Dynamic Virtual Bats Algorithm”, Information Sciences 354 (2016) 222–235.

[14] Xin-She Yang, “Bat algorithm: literature review and applications”, Int. J. Bio-Inspired Computation, Vol. 5, No. 3, pp. 141–149 (2013). DOI: 10.1504/IJBIC.2013.055093.

[15] Bahriye Akay, “A study on particle swarm optimization and artificial bee colony algorithms for multilevel thresholding”, Applied Soft Computing 13 (2013) 3066–3091.

[16] Kai Chen, Yifan Zhou, Zhisheng Zhang, Min Dai, Yuan Chao, and Jinfei Shi, “Multilevel Image Segmentation Based on an Improved Firefly Algorithm”, Hindawi Publishing Corporation Mathematical Problems in Engineering, Volume 2016, Article ID 1578056, 12 pages.

[17] Adis Alihodzic and Milan Tuba, “Improved Hybridized Bat Algorithm for Global Numerical Optimization”, 2014 UKSim-AMSS 16th International Conference on Computer Modelling and Simulation.

[18] Rainer Storn and Kenneth Price, “Differential Evolution – A Simple and Efficient Heuristic for Global Optimization over Continuous Spaces”, Journal of Global Optimization 11**:** 341–359, 1997.

[19] Xin-She Yang, “Nature-Inspired Metaheuristic Algorithm”, Luniver Press, UK in 2010.

[20] Nandita Sanyal, Amitava Chatterjee and Sugata Munshi, “An adaptive bacterial foraging algorithm for fuzzy entropy based image segmentation”, Expert Systems with Applications 38 (2011) 15489–15498.

[21] A. De Luca and S. Termini, “A Definition of a Nonprobabilistic Entropy in the Setting of Fuzzy Sets Theory”, Information and Control *20*, 301--312 (1972).

[22] Wen-Bing Tao, Jin-Wen Tian and Jian Liu, “Image segmentation by three-level thresholding based on maximum fuzzy entropy and genetic algorithm”, Pattern Recognition Letters 24 (2003) 3069–3078.

[23] Wenbing Tao, Hai Jin and Liman Liu, “Object segmentation using ant colony optimization algorithm and fuzzy entropy”, Pattern Recognition Letters 28 (2007) 788‑796.

[24] Mansuo Zhao, Alan M. N. Fu, and Hong Yan, "A Technique of Three-Level Thresholding Based on Probability Partition and Fuzzy 3-Partition", IEEE Transactions on Fuzzy Systems, Vol. 9, No. 3, June 2001.

[25] H. D. Cheng, C. H. Chen, H. H. Chiu, and Huijuan Xu, "Fuzzy Homogeneity Approach to Multilevel Thresholding", IEEE Transactions on Image Processing, Vol. 7, No. 7, July 1998.

[26] H.D. Cheng, Yen-Hung Chen and Ying Sun, "A novel fuzzy entropy approach to image enhancement and thresholding", Signal Processing 75 (1999) 277-301.

[27] H. D. Cheng, Y. H. Chen, and X. H. Jiang, "Thresholding Using Two-Dimensional Histogram and Fuzzy Entropy Principle", IEEE Transactions on Image Processing, Vol. 9, No. 4, April 2000.

[28] Linda Mahmoudi and Ali El Zaart, "A Survey of Entropy Image Thresholding Techniques", 2012 22nd International Conference on Advances in Computational Tools for Engineering Applications (ACTEA).

[29] P. K. Sahoo, S. Soltani, and A. K. C. Wong, "A Survey of Thresholding Techniques", Computer Vision, Graphics, and Image Processing 41, 233-260 (1988).

[30] Madhubanti Maitra and Amitava Chatterjee, "A novel technique for multilevel optimal magnetic resonance brain image thresholding using bacterial foraging", Measurement 41 (2008) 1124–1134.

[31] Xin-She Yang, "Harmony Search as a Metaheuristic Algorithm", in: Music-Inspired Harmony Search Algorithm: Theory and Applications (Editor Z. W. Geem), Studies in Computational Intelligence, Springer Berlin, vol. 191, pp. 1-14 (2009).

[32] G.-Q. Huang, W.-J. Zhao, and Q.-Q. Lu, "Bat algorithm with global convergence for solving large-scale optimization problem," Application Research of Computers, vol. 30, no. 5, pp. 1323–1328, 2013.

[33] K. Khan, A.Nikov, and A. Sahai, "A fuzzy bat clustering method for ergonomic screening of office workplaces," in Advances in Intelligent and Soft Computing, vol. 101, pp. 59–66, Springer,2011.

[34] L. Jiann-Horng, C. Chao-Wei, Y. Chorng-Horng, and T. Hsien-Leing, "A chaotic levy-flight bat algorithm for parameter estimation in nonlinear dynamic biological systems," Journal of Computer and Information Technology, vol. 2, no. 2, pp. 56–63, 2012.

[35] J. Zhang and G. Wang, “Image matching using a bat algorithm with mutation,” Applied Mechanics and Materials, vol. 203, no.1, pp. 88–93, 2012.

[36] N. Otsu, “A threshold selection method for grey level histograms,” IEEE Transactions on Systems, Man and Cybernetics, vol. 9, no. 1, pp. 62–66, 1979.

[37] T. Pun, “Anewmethod for grey-level picture thresholding using the entropy of the histogram,” Signal Processing, vol. 2, no. 3, pp. 223–237, 1980.

[38] T. Chaira and A. K. Ray, “Threshold selection using fuzzy set theory,” Pattern Recognition Letters, vol. 25, no. 8, pp. 865–874, 2004.

[39] T. Chaira and A. K. Ray, “Segmentation using fuzzy divergence,” Pattern Recognition Letters, vol. 24, no. 12, pp. 1837–1844, 2003.

[40] T. Pun, “Entropic thresholding: A new approach”, Comput. Vision Graphics Zmage Process. 16, pp. 210-239, 1981.

[41] T. Pun, “A new method for gray-level picture thresholding using the entropy of the histogram”, Signal Process. 2, pp. 223-237, 1980.

[42] J.C. Yen, F.J. Chang, , S. Chang, “A new criterion for automatic multilevel thresholding”, IEEE Trans. on Image Processing, IP-4, pp. 370-378, 1995.

[43] G. Johannsen and J. Bille, “A threshold selection method using information measures”, in Proceedings, 6th Znt. Conf. Pattern Recognition, Munich, Germany, pp. 140-143, 1982.

[44] P. Sahoo, *et al*., “Threshold Selection using Renyi’s Entropy”, Pattern Recognition, vol. 30, no 1, 1997.

[45] C.A.B. Mello, *et al*. “Image Thresholding of Historical Documents: Application to the Joaquim Nabuco's File”, Eva Vienna, pp. 115-122, Austria, 2006.

[46] J.M. Silva, *et al.*, “Binarizing and filtering historical documents with back-to-front interference”, Proceedings of the ACM SAC, France, 2006.

[47] S. Kullback,: “Information theory and statistics”, Dover, 1968.

[48] C. Li, and P. Tam, “An Iterative Algorithm Cross Entropy Thresholding,” Pattern Recognition Letter - Elsevier, vol.19, no. 8, pp. 771-776, 1998.

[49] R. Al-Attas, and A. El-Zaart, “Thresholding of Medical Images Using Minimum Cross Entropy”, Kuala Lumpur international conference on biomedical engineering, pp. 312-315, Kuala Lumpur, Malaysia, 2006.

[50] G. Al-Osaimi and A. El Zaart, “Minimum Cross Entropy Thresholding for SAR Images”, 3rd IEEE International Conference on Information & Communication Technologies: From Theory to Applications ICTTA. Syria, April 2008.

[51] D. Al-Saeed and A. El Zaart, “Minimum Cross Entropy Thresholding Using Entropy-Li Based on Log-normal Distribution for Skin Cancer Images”, Seventh International Conference on Signal Image Technology & Internet-Based Systems, 2011.

[52] A. Brink, and N. Pendock, “Minimum Cross-entropy Threshold Selection,” Pattern Recognition Letter - Elsevier, vol. 29, no. 1, pp. 179-188, 1996.

[53] N.R. Pal, “On Minimum Cross-Entropy Thresholding”, Pattern Recognition Journal Elsevier, vol.29, no. 4, pp. 575-580, 1996.

[54] A. Al-Ajlanand A. El Zaart, “Minimum Cross Entropy Thresholding Using Gamma Distribution”, 3rd IEEE International Conference on Information & Communication Technologies: From Theory to Applications ICTTA. Syria, April 2010.

[55] A.G. Shanbag, “Utilization of Information Measure as a Means of Image Thresholding”, Computer Vision Graphics and Image Processing, 56, pp. 414-419,1994.

[56] R. C. Gonzalez and R. E. Woods, “Digital Image Processing”, Pearson Education, 2008.

[57] C.P. Loizou, S. Petroudi, I. Seimenis, M. Pantziaris and C.S. Pattichis. “Quantitative Texture Analysis of Brain White Matter Lesions Derived from T2-Weighted MR Images in MS Patients with Clinically Isolated Syndrome”. Journal of Neuroradiology (2014), 1-16.

[58] C.P. Loizou, V. Murray, M.S. Pattichis, I. Seimenis, M. Pantziaris, C.S. Pattichis, “Multi-scale amplitude modulation-frequency modulation (AM-FM) texture analysis of multiple sclerosis in brain MRI images,” IEEE Trans. Inform. Tech. Biomed., vol. 15, no. 1, pp. 119-129, 2011.

[59] C.P. Loizou, E.C. Kyriacou, I. Seimenis, M. Pantziaris, S. Petroudi, M. Karaolis, C.S. Pattichis, “Brain white matter lesion classification in multiple sclerosis subjects for the prognosis of future disability,” Intelligent Decision Technologies Journal (IDT), vol. 7, pp. 3-10, 2013.

[60] C.P. Loizou, M. Pantziaris, C.S. Pattichis, I. Seimenis, “Brain MRI Image normalization in texture analysis of multiple sclerosis”, J. Biomed. Graph. & Comput., vol. 3, no.1, pp. 20-34, 2013.

CHAPTER 4

MICROCONTROLLER BASED COMMUNICATION SYSTEM FOR APPLICATIONS IN TELEHEALTH

4.1 Introduction

Telehealth is the use of telecommunication and information technologies for the delivery of health-related services and information. Telehealth encompasses preventative, promotive and curative aspects. In the context of the present work, after successfully obtaining the brain MRI segments, they are forwarded to a medical practitioner who may not be present at the site, for the purpose of proper diagnosis or prognosis of the concerned patient. Hence in this chapter, a dedicated microcontroller based communication system has been developed which will cater to the above needs and thus can be used for telehealth purposes. The benefits of this system over conventional emailing are manifold. Firstly, in this system stored data as well as real time data can be transferred within a distributed environment like a hospital or a diagnostic center making use of the already existing LAN infrastructure without depending on the main server, thus enhancing the reliability. Secondly, the LAN when connected to the internet may enable the data to be available even beyond the domain of LAN and from anywhere across the globe. Thirdly, availability of the data and the extent of security is defined by the sole discretion of the system designer and working personnel. And finally, the developed system also provides the user with the flexibility to send only those portions of the huge segmented MRI data which are of interest to the medical practitioner, thus making optimum use of the communication resources.

4.2 Overview of the present scheme

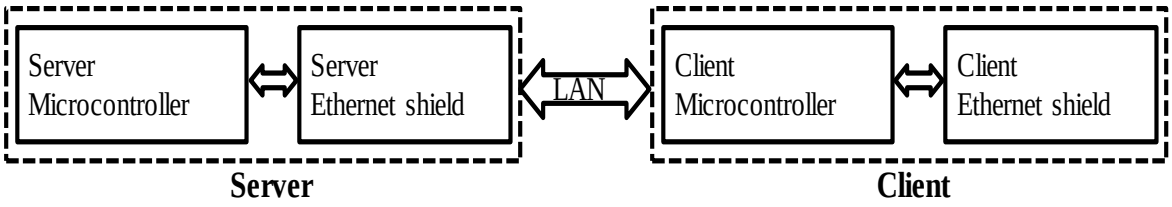

Fig 4.1 Schematic block diagram of proposed scheme

The present scheme, as shown in Fig-4.1, consists of two microcontrollers each of which is connected to an Ethernet shield. One microcontroller in conjunction with its Ethernet shield acts as a server to transmit data into the LAN. The server microcontroller, apart from its mere role as a server can collect data through anyone or combination of the following methods:

(i) Collecting real-time data through analog ports coupled with in-built ADCs.

(ii) Collecting real-time data through Digitals ports.

(ii) Storing data within in-built memories first and then collecting them when necessary.

The server microcontroller first configures the Ethernet shield as a server and assigns a particular IP to it. Then the microcontroller sends data to the server Ethernet shield for transmitting the same into LAN.

On the other side of the LAN, there is another microcontroller coupled with a separate Ethernet shield. This setup is called client. The Ethernet shield is configured by its associated microcontroller as client and another IP address is specified for this. The client shield makes a call to the server by floating the appropriate IP address of the server, get accesses over data and the received data is sent to the client microcontroller. The client microcontroller, upon receiving the data, can do anyone of the following things:

(i) Sends data through its digital ports.

(ii) Stores data into in-built memories.

4.3 Hardware and its overview

Each of the two microcontrollers, stated here as server microcontroller and client microcontroller, is basically mounted within a Mega2560 board R3 ™ with ATmega2560 processor as its heart. This is shown in Fig-4.2. Its technical specification is given in Table-4.1.

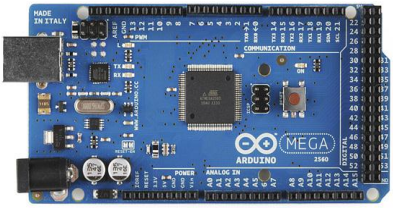

Fig: 4.2

Fig: 4.3

Microcontroller	ATmega2560
Operating Voltage	5V
Input Voltage (recommended)	7-12V
Input Voltage (limit)	6-20V
Digital I/O Pins	54 (of which 15 provide PWM output)
Analog Input Pins	16
DC Current per I/O Pin	20 mA
DC Current for 3.3V Pin	50 mA
Flash Memory	256 KB of which 8 KB used by bootloader

SRAM	8 KB
EEPROM	4 KB
Clock Speed	16 MHz

Table-4.1: Technical specification of ATmega 2560.

The Mega 2560 can be powered via the USB connection or with an external power supply. The power source is selected automatically. In present case, the USB cable connected to the computer is used to power up the board and at the same time is utilized to program the board from PC as well.

Each of the two Ethernet shields of model W5100, specified here as server shield and client shield, acts as an attachment of the corresponding microcontroller. This is shown in Fig-4.3. Its technical specification is given in Table-4.2.

Micro SD interface 5V/3.3V double operational voltage level 10Mb/100Mb Ethernet socket with POE All electronic brick interfaces are broken out Operation temperature: -40℃ ~ +85℃ The shield contains a number of informational LEDs: • PWR: indicates that the board and shield are powered • LINK: indicates the presence of a network link and flashes when the shield transmits or receives data • FULLD: indicates that the network connection is full duplex • 100M: indicates the presence of a 100 Mb/s network connection (as opposed to 10 Mb/s) • RX: flashes when the shield receives data • TX: flashes when the shield sends data • COLL: flashes when network collisions are detected

Table-4.2: Technical specification of W5100 Ethernet shield.

The shield is attached with the microcontroller board with pin-to-pin plugging connection. This Ethernet module is connected to the network via one RJ45 cable through which actual data transfer takes place between the shield module and the network.

4.4 Software Implementation

A program is written in ARDUINO software environment installed on PC. This program has two working parts:

(i) A part that is used to configure the Ethernet shield via the microcontroller.

(ii) Another part that takes care of online transmission of data between microcontroller and shield as well as between network and shield.

Any program in ARDUINO environment is called a sketch and structurally contains two parts:

(i) A `setup()` part of sketch that defines

(a) The `mac` address of the Ethernet device.

(b) The IP Address, Gateway, subnet and port address that the shield has to use for network access.

For client shield, IP Address of server is specified so that the client can search that particular server.

(ii) A `loop()` part of sketch that is used

(a) At the server end to check if any client is connected and available.

1. If the client is available and connected, character stream is received from client.

2. If a newline character followed by a blank line is received, a standard http request is sent to the client.
3. A stream of data is sent to the client followed by a particular terminating character ('%' is used in present case).
4. The client is disconnected.
5. A small delay (1 ms in present case) is introduced at the end to offer a tolerance in time for accessing the data from the client end.

The loop will be repeated.

(b) At the client end to check if the particular server is connected.

1. If the particular server is available, the client reads the data from server.
2. The data with particular terminating character ('%' in present case) is received and displayed through serial monitor of the PC connected to the client.

The loop will be repeated.

4.5 Experimental Results

The work has been conducted in the *store-and-forward* mode in three stages. First the linear indices of the segmented binary images have been extracted and compiled as a text file. This text file is then transmitted by the proposed communication scheme and finally the original image has been reconstructed. The extraction and reconstruction has been done with the help of simple MATLAB® programs.

The server containing microcontroller and Ethernet shield under actual working condition is shown in Fig-4.4.

The client containing microcontroller and Ethernet shield under actual working condition and connected to PC is shown in Fig-4.5. An exaggerated view of the microcontroller and the Ethernet shield with PC-USB cable terminal and RJ45 cable terminal is shown in Fig-4.6. The arrangement collects data from LAN and transmits them serially to the PC. Finally, the data is displayed in the monitor of the PC. The entire arrangement at the client end with real time display of data is shown in Fig-4.7 and 4.8.

Fig: 4.4

Fig: 4.5

Fig: 4.6

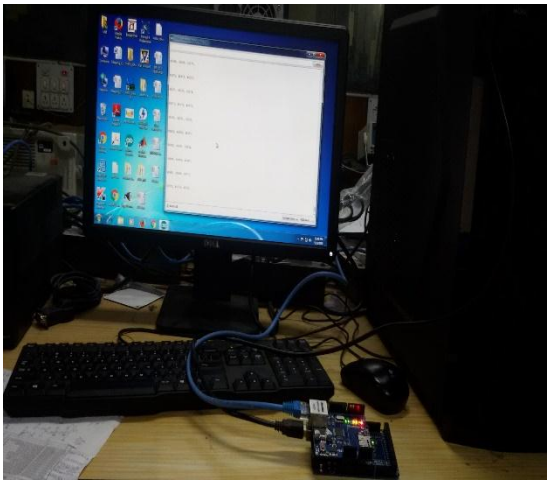

Fig: 4.7

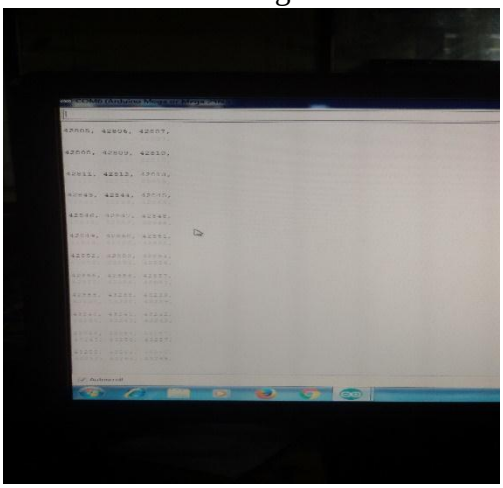

Fig: 4.8

After receiving the data points, the images have been reconstructed. The reconstruction results have been shown in Fig 4.9.

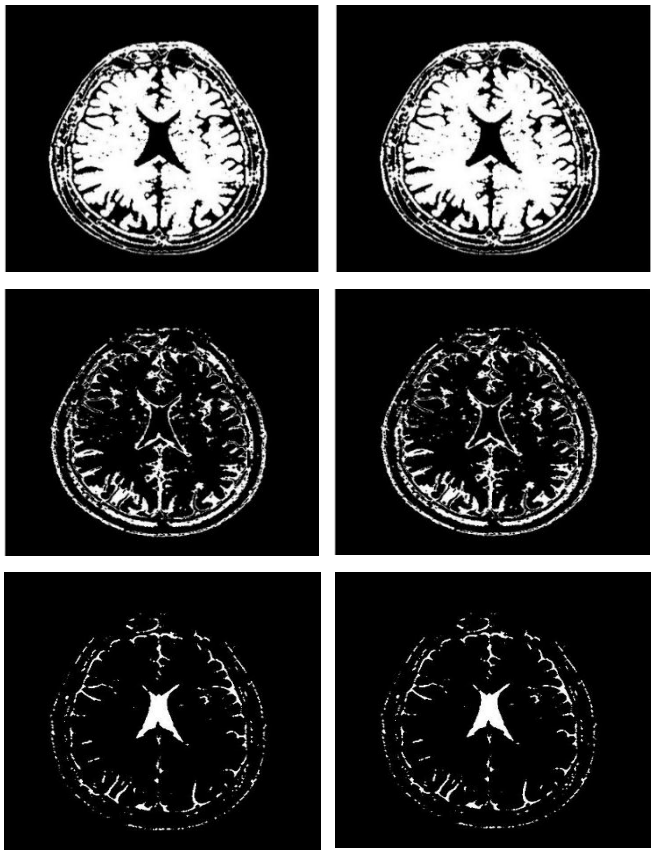

Fig 4.9 1st column: Sent segmented images

2nd column: Received segmented images

4.6 Conclusions

In this chapter a microcontroller based communication system has been devised which is capable of online transmission of the segmented binary images for applications in telehealth. The advantage of the present work using LAN as the medium of transmission of data is manifold and has far-reaching consequences. The data, once collected from patient at test center, is fed to a server microcontroller that transmits it eventually through the existing infrastructure of network anywhere within the premises of a particular hospital or diagnostic center. The doctor or an appropriate person having expertise in the related field with a capability of supervising the condition of the patient can have an access over the test data of the patient at any point of time

from any position within the domain of the network without being present physically at the site of investigation. The client apparatus being portable may be carried easily across the premises and consequently be connected to a PC or laptop for accessing the data. This also reduces the delay in propagation of information by any other means which otherwise may be detrimental to the condition of the patient. The online availability of the data from managerial or administrative level may enable them to process the data from other angles suitable for arranging and running the system appropriately. Moreover, the data prevailing in the network may be uploaded beyond the domain of the intra-network of the organization by the main server as a result of which, the data could be accessed outside the network, anywhere across the globe via internet. However, this method of launching data beyond the existing network of the organization has not been implemented although the promise of such possibility is evident from the experience on outcome of the experiment.

CHAPTER 5

CONCLUSIONS AND FUTURE WORK

5.1 Conclusions

In this thesis, some image processing techniques have been studied for the purpose of obtaining satisfactory segmentation of MR images of the human brain. The image processing techniques under study encompasses two distinct methods. The first method is a mathematical morphology aided image enhancement technique, followed by fuzzy clustering as discussed in Chapter 2. The second method is a comparatively recent metaheuristic algorithm i.e., the Bat Algorithm (BA) utilized for optimal multilevel thresholding, as discussed in Chapter 3. Moreover, in Chapter 4, a microcontroller based communication system has been developed which enables the user to transfer the required segmented images to an offsite medical practitioner according to his/her needs.

In Chapter 2, the proposed image enhancement technique based on the concepts of mathematical morphology, coupled with Fuzzy C-means (FCM) clustering have resulted in a better segmentation of the brain MR images in comparison to the case where FCM is directly applied to the raw, unprocessed MR images. This is evident from the better values of partition coefficient and partition entropy which have been selected as the cluster validity functions.

In Chapter 3, the bat algorithm in its basic form has been applied to obtain multilevel optimal thresholding-based segmentation of the brain MR images. Fuzzy entropy of the image histogram has been chosen as the objective function. Due to unsatisfactory performance of this basic BA, a venture has been made in order to develop a Modified Hybridized Bat Algorithm (MHBA) which has increased the exploration capability of the solutions in the multi-dimensional search space and resulted in more optimally thresholded MR images. Thus, better values have been obtained for both the objective function as well as the uniformity measure, on application of MHBA.

Finally, in Chapter 4, the binary image segments obtained from the methods discussed in Chapter 2 and 3, have been transmitted from the source computer to a destination computer with the help

of a microcontroller based communication system, utilizing the existing LAN. This has been done for potential applications in the domain of telehealth.

5.2 Future scope of work

The future scopes of work are many and spans a variety of applications. The proposed image segmentation methods can be studied and adopted for a wide range of medical images apart from brain MRI, as well as for various other types of images. A different combination of the morphological operators involving a variety of structuring elements, differing in size and shape can also be brought under the scope of further study for the purpose of image enhancement. Other recent metaheuristics algorithms like the Firefly Algorithm (FA), Cuckoo Search (CS) algorithms etc. may also be studied as a means of achieving optimal multilevel thresholding-based segmentation of the images. Additionally, the entire concept of these segmentation techniques can be applied to 1-D signals as well. Moreover, in case of the proposed communication system, an attempt can be made to practically implement the concept of data transmission beyond the domain of LAN. There is also a scope of real time data transfer which can be further investigated employing the proposed microcontroller based communication method.